VI. APPLIED PLASMA RESEARCH

A. Active Plasma Systems

Academic Research Staff

Prof. L. D. Smullin
Prof. A. Bers
Prof. R. R. Parker
Prof. K. I. Thomassen

Graduate Students

N. J. Fisch
S. P. Hirshman
C. F. F. Karney
J. L. Kulp
R. K. Linford
G. H. Neilson
J. J. Schuss
M. D. Simonutti
M. S. Tekula
A. L. Throop
D. C. Watson
P. R. Widing

1. DISPERSION RELATIONS (WAVE NUMBER vs DENSITY) FOR WARM-PLASMA MODES NEAR LOWER HYBRID RESONANCE

National Science Foundation (Grant GK-28282X1)

M. D. Simonutti, R. R. Parker

Fundamental to understanding lower hybrid resonance (LHR) of waves in plasmas is an analysis of the linear dispersion relation of these waves. The dispersion relations analyzed here are obtained from linear, cold-plasma theory, and from the linearized moment equations in the electrostatic approximation. We consider an electron-ion plasma with a single ion species, and we do not treat nonlinear effects.

The physical situation of interest is the coupling of RF power to a plasma from an antenna located at the outer edge of a plasma column out of the main body of the plasma. The RF power passes through a region of increasing plasma density by means of a long wavelength or cold-plasma mode and, with the local wavelength steadily decreasing, approaches the LHR density layer. Linear warm-plasma theory predicts that the wave converts from the cold-plasma mode to a short wavelength mode before reaching the LHR density, and this mode directs the RF power back toward the outside of the plasma column. The wavelength continues to decrease until strong collisionless damping mechanisms can convert the RF wave energy into particle random kinetic energy, and hence heat the plasma.

Many workers have studied the problem of linear mode conversion in inhomogeneous media, especially as it applies to wave conversion near LHR in a region of increasing density. The first statement and treatment of this problem is in the well-known paper by Stix.[1] Linear mode conversion analysis involves dealing with a linear differential equation with spatially varying coefficients which describes wave propagation in a plasma of nonuniform density. The results of that approach, although interesting, are restricted

because a wide range of parameters of interest cannot easily be included.

Considerable insight into the problem can be gained through a study of the homogeneous plasma dispersion relation as a function of density and for different sets of parameters. The density at which mode conversion takes place and the magnitude of the local wavelength and group velocity can be determined from this study. Although this is a relatively straightforward task, such a comprehensive study has not been previously reported.

Analysis of the dispersion relation vs density for various sets of parameters of interest is difficult if results are required in analytic form. Glagolev[2] has published this kind of analysis, in which he was forced to make many approximations. We have found that his results are not accurate in some parameter ranges of interest to us. We have taken a numerical, rather than a purely analytical, approach to the problem. Although our analysis has the disadvantages common to numerical studies, we consider its conclusions accurate and interesting.

Computer programs have been prepared that evaluate, over a density range from zero to beyond the hybrid resonant density, the wave number in the direction of inhomogeneity and the group velocity of modes of propagation as determined by linear cold-plasma theory and by the linearized moment equations in the electrostatic approximation.

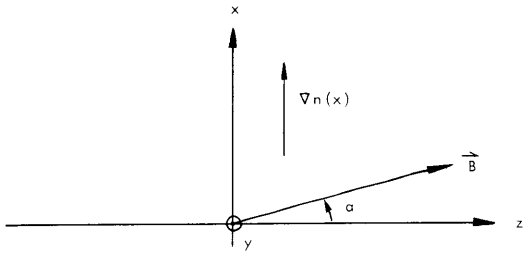

Fig. VI-1.
Rectangular coordinate geometry.

The rectangular coordinate geometry of the problem is indicated in Fig. VI-1. The density gradient is solely in the x direction and, therefore, the y-z plane is parallel to the surfaces of constant density. In this analysis the uniform magnetic field, usually taken as exactly parallel to the surfaces of constant density, is not under that constraint. The magnetic field direction vector is in the x-z plane and at an angle α to the z axis; therefore, the magnetic field is at an angle α to the constant density surfaces. The x direction is the only direction of inhomogeneity, and this allows the y and z coordinates to be transformed by Fourier analysis. Space-time variation of the modes is taken as $\exp(i(\omega t - \bar{k} \cdot \bar{r}))$, where $\bar{k} = k_x \vec{i}_x + k_y \vec{i}_y + k_z \vec{i}_z$.

The input parameters for the program are relative wave numbers $n_y = \frac{k_y}{\omega/c}$, and

$n_z = \frac{k_z}{\omega/c}$, ion and electron temperatures, ion mass, and ω_{ce}/ω, where $\omega_{ce} = \frac{e|B|}{m_e}$. The last two parameters determine the density of LHR, provided that the inequality $\frac{m_i}{m_e} > \frac{\omega_{ce}}{\omega} > \left(\frac{m_i}{m_e}\right)^{1/2}$ holds. The program calculates the $n_x = \frac{k_x}{\omega/c}$ solutions and the inverse group velocities c/v_{gx}, c/v_{gy}, c/v_{gz} for densities zero to beyond the LHR density.

We present here results for a hydrogen plasma with ω_{ce}/ω fixed at 50, and this corresponds to a value for ω_{pe}/ω_{ce} of ~1.7 at the LHR density. This is representative of the planned M.I.T. Alcator lower hybrid heating experiment and of a small wave-measurement experiment. Figure VI-2 indicates the general nature of the dispersion relation with mode conversion from thermal effects and also contrasts this with the cold-plasma dispersion relation, which displays a true resonance at the LHR density. Curves are given for several plasma temperatures.

We note that the warm-plasma mode determined by the moment equations in the electrostatic approximation makes a smooth transition from the cold-plasma electromagnetic

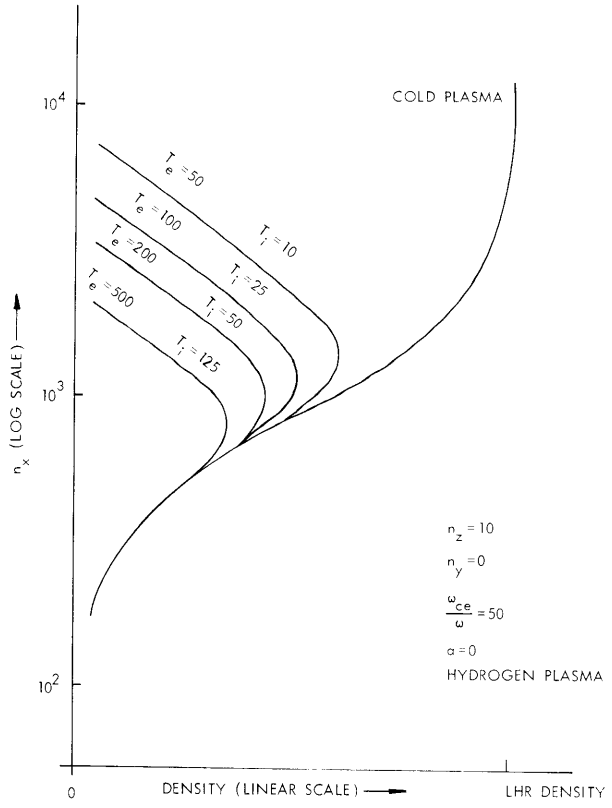

Fig. VI-2. n_x vs density with plasma temperature as a parameter.

mode as density increases, thereby indicating that the electrostatic character of the mode begins to dominate before the thermal effects come into play. The warm-plasma curves have two solutions for n_x at a given density. Physically, the interpretation is that a wave would be launched into the plasma via the smaller n_x mode, which increases as the wave goes to higher densities. At the conversion point the x-directed group velocity of the mode goes through zero, changes sign, and sends the RF power back toward the outside of the plasma. There is continued increase in n_x until collisionless damping of the wave takes place. Of course, the moment-equation dispersion relations, and therefore the curves presented here, do not show this collisionless damping.

We note in Fig. VI-2 that the wave conversion density decreases from the LHR density as the plasma temperature increases. For the given curves the density changes by approximately a factor of two. Although it is not explained here, it has been shown that relative increases in either T_e or T_i contribute approximately equally in this effect.

In Fig. VI-3 the plasma temperature is kept fixed and the parameter n_z is varied. As n_z is increased, the wave conversion density again decreases from the LHR density. Figures VI-2 and VI-3 indicate that the longer wavelength mode is strongly dependent

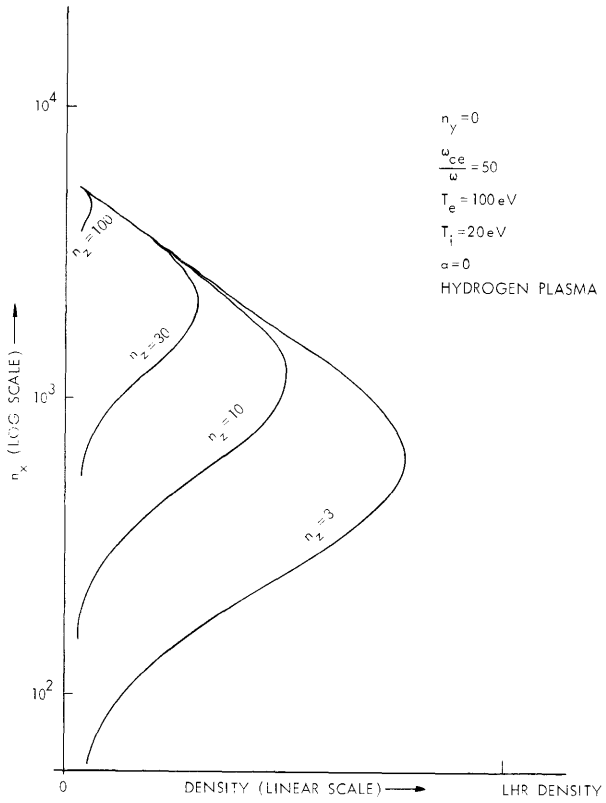

Fig. VI-3. n_x vs density with n_z as a parameter.

on n_z rather than on temperature, while the reverse is true for the shorter wavelength mode; n_y has very little effect on these dispersion relations for the n_y range of interest.

For the case $a = 0$, which is the most commonly considered, the dispersion relation is a function of n_x^2. Therefore, the curves in this case correspond to modes with n_x both positive and negative with the magnitude given. Also, these curves correspond to pure real values for n_x. For densities beyond the wave conversion density, roots for n_x are complex, which indicates that there is no propagation for that region. We have not plotted complex n_x.

In Fig. VI-4 the dispersion relation (the n_x curve) is plotted against density for a sample set of parameters along with the x and z inverse group velocities corresponding

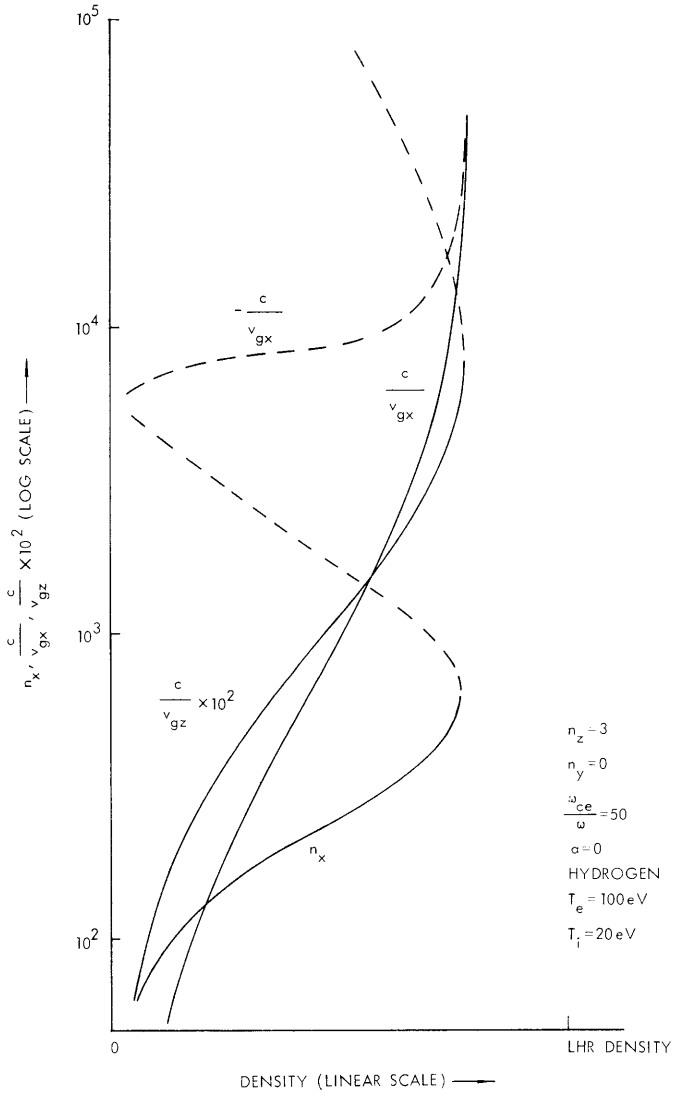

Fig. VI-4. n_x, $\frac{c}{v_{gx}}$, $\frac{c}{v_{gz}}$ vs density.

to that dispersion relation. (The group velocity in the y direction is zero because the condition $n_y = 0$ was taken.) The solid lines correspond to the long wavelength mode up to the conversion point, the dashed lines correspond to the short wavelength mode. The variable of inverse group velocity normalized by the speed of light was chosen for presentation because n_x is essentially the inverse phase velocity normalized by c.

Since the x-directed group velocity goes through zero and changes sign at the wave conversion point, the longer wavelength mode, for the x direction, is a backward wave, that is, one whose phase and group velocities are oppositely directed.

The z-directed group velocity is continuous and continually decreases in going from the longer to the shorter wavelength mode. This group velocity is considerably greater than that in the x direction; therefore, the RF power flows nearly parallel to the z direction.

Figure VI-5 shows results for nonzero α, which corresponds to obliqueness between the density gradient and the magnetic field. It is well known that this condition has significant bearing on the propagation of waves in the ionosphere, but this has not been

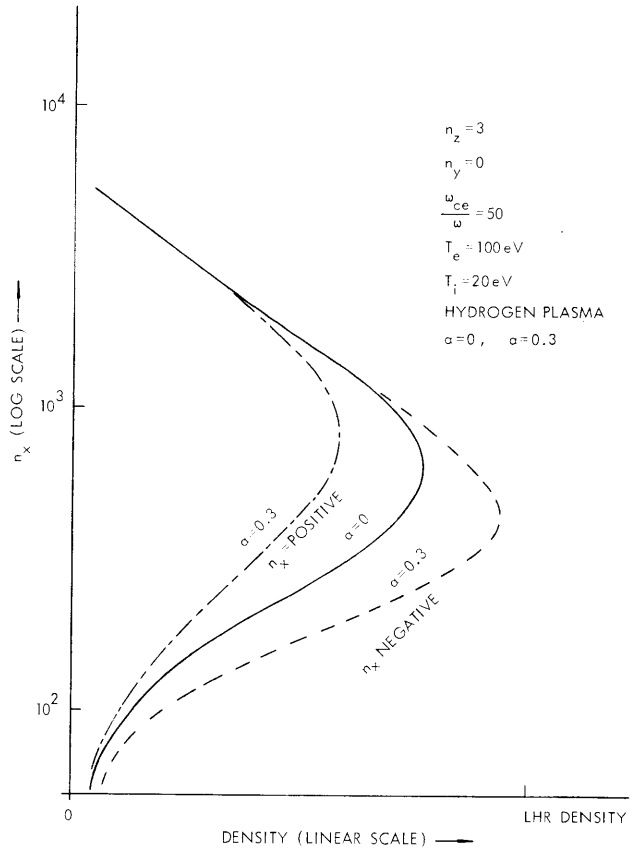

Fig. VI-5. n_x vs density for $\alpha = 0$ and $\alpha = 0.3$ degrees.

established experimentally for laboratory plasmas.

For the case $\alpha \neq 0$, the dispersion relation is a function of n_x rather than of n_x^2. Therefore the solutions for n_x no longer occur in a pair of equal magnitude and opposite signs. Instead, the result appears in Fig. VI-5, where the plus and minus branches of n_x are of different magnitude at a given density. Figure VI-5 also shows the $\alpha = 0$ dispersion relation for the same values of the other parameters n_z, T_e, etc. If the sign of the product $n_z \sin \alpha$ is changed, then the signs of the plus and minus n_x curves in Fig. VI-5 are interchanged.

We are interested in the physical situation with the RF power entering the plasma via the longer wavelength mode. Therefore, for nonzero α, the wave conversion density becomes greater or less than that for the $\alpha = 0$ case, depending on the sign of $n_z \sin \alpha$. In a laboratory experiment the n_z excitation spectrum would normally include both positive and negative n_z components.

Conclusion

We now have a means of determining actual magnitudes of important variables, such as the wave conversion density, local wavelength, and group velocity, for modes of interest in designing an LHR scheme based on linear theory. Of course, much more information is required in order to use these results. The limitations of Landau damping and finite Larmor radius effects must be kept in mind. An experimental RF antenna of finite n_z extent would excite a spectrum of n_z modes. This results in a field distribution that is the warm-plasma counterpart of the cold-plasma resonance cone effect.[3-5] This poses a problem whose solution would be most interesting but very difficult; that is, to describe the resonance cone structure in a warm inhomogeneous plasma.

One conclusion that can be drawn directly from these results is that LHR heating based on the wave conversion principle cannot be applied to a laboratory experiment of only modest density and magnetic field. The key to this lies in Fig. VI-3, which indicates the effect of the parameter n_z. Low density and magnetic field imply that the RF generator has a low LHR frequency ω. Moderately sized laboratory plasmas imply a limited length for the RF antenna in the plasma and, therefore, a broad spectrum of k_z excited by this antenna. Since $n_z = k_z c/\omega$, most of the n_z spectrum can lie well beyond $n_z = 10^3$. Figure VI-3 suggests that at such large n_z, the wave conversion type of mode no longer exists. We do not show this, but we state that at high n_z and/or T_e and T_i the modes become ion-acoustic in nature. These modes are very insensitive to density and are difficult to excite from an antenna outside of the plasma column. Thus the wave-conversion mechanism does not come into play.

References

1. T. H. Stix, "Radiation and Absorption via Mode Conversion in an Inhomogeneous Collision-Free Plasma," Phys. Rev. Letters 15, 878 (1965).
2. V. M. Glagolev, "Propagation and Absorption of Hybrid Waves in a Weakly Inhomogeneous Plasma Layer – I," Plasma Phys. 14, 301-314 (1972).
3. R. R. Parker, "Alcator Lower Hybrid-Heating Experiment," Quarterly Progress Report No. 102, Research Laboratory of Electronics, M.I.T., July 15, 1971, pp. 97-111.
4. M. Simonutti, R. R. Parker, and R. J. Briggs, "Observation of Wave Propagation in a Magnetized Plasma near the Lower Hybrid Resonance," Quarterly Progress Report No. 104, Research Laboratory of Electronics, M.I.T., January 15, 1972, pp. 196-201.
5. M. Simonutti, R. R. Parker, and R. J. Briggs, "Effect of Obliqueness between Density Gradient and Magnetic Field on Resonance Cones near the Lower Hybrid Resonance," Quarterly Progress Report No. 105, Research Laboratory of Electronics, M.I.T., April 15, 1972, pp. 105-109.

2. SYMBOLIC COMPUTATION OF NONLINEAR WAVE-WAVE INTERACTIONS

National Science Foundation (Grant GK-28282X1)

J. L. Kulp, C. F. F. Karney, A. Bers

A previous report[1] described the general capabilities of the MACSYMA system for use in plasma physics, and gave a plan for the study of coherent nonlinear wave coupling in a two-fluid plasma model. In this report we present some of the techniques that have been developed and new problems that have been identified. The physical results are given in Sec. VI-A.3.

Techniques for Derivation of the Nonlinear Current

It is convenient to think of the derivation and evaluation of the nonlinear current $\bar{J}^{(2)}$ as separate steps. The first operation in the derivation of $\bar{J}^{(2)}$ is to expand the nonlinear fluid equations in the electric field amplitude. A function EXPEQS has been developed for this purpose. It takes as arguments: (i) a list of equations or expressions to be expanded; (ii) a list of variables, functional forms, or subscripted variables to be expanded in a power series in the expansion parameter; (iii) lowest order equations to be kept; and (iv) highest order equations to be kept. The expansion parameter is arbitrary and can be set to any variable. Options exist for controlling the structuring of the resulting equations. Usually the equations are put in a form such that higher order variables (v_2, n_2, etc.) are driven by lower order ones (v_1, n_1, E, etc.). Typically expansions are one of the easiest tasks for symbolic manipulation systems to carry out. The

An example of the use of the EXPEQS function in the expansion of fluid equations:

```
(C5) LOADFILE(LFUNS,EXPQ,DSK,BERS)$

LFUNS EXPQ DSK BERS BEING LOADED
LOADING DONE

(C6) BATCH(EQS,FLUID,DSK,PLASMA)$

(C6) (MAKENONSCALAR(V,N,E,B), DOTNONASSOC:TRUE,
?MPUTPROP(GRAD,TRUE,DOTOPERATOR),?MPUTPROP(XPDT,TRUE,DOTOPERATOR),
?MPUTPROP(D,''?CDR([DOTOPERATOR]),?ARRAYPROPS))$
```

The fluid force equation:

```
(C7) FORCE:N*D[T].V + N*(V.GRAD).V + (VTH^2)*GRAD.N = N*(Q/M)*E + N*(Q/M)*V.XPDT.B;
```

(D7) $$N\,(D_T \cdot V) + N\,((V \cdot \mathrm{GRAD}) \cdot V) + (\mathrm{GRAD} \cdot N)\,\mathrm{VTH}^2 = \frac{E\,N\,Q}{M} + \frac{N\,Q\,(V \cdot (\mathrm{XPDT} \cdot B))}{M}$$

The continuity equation:

```
(C8) CONS:D[T].N + GRAD.(N.V) = 0;
```

(D8) $$\mathrm{GRAD} \cdot (N \cdot V) + D_T \cdot N = 0$$

Expansion to third order in an arbitrary parameter. (Could be the electric field)

```
(C10) EQS:EXPEQS([FORCE,CONS],[V,N,E,B],0,3);
```

(E10) $$NO\,(D_T \cdot VO) - \frac{NO\,Q\,(VO \cdot (\mathrm{XPDT} \cdot BO))}{M} + NO\,((VO \cdot \mathrm{GRAD}) \cdot VO) = \frac{EO\,NO\,Q}{M} - (\mathrm{GRAD} \cdot NO)\,\mathrm{VTH}^2$$

(E11) $$\mathrm{GRAD} \cdot (NO \cdot VO) + D_T \cdot NO = 0$$

(E12) $$NO\,(D_T \cdot V1) + NO\,((VO \cdot \mathrm{GRAD}) \cdot V1) - \frac{NO\,Q\,(V1 \cdot (\mathrm{XPDT} \cdot BO))}{M} + NO\,((V1 \cdot \mathrm{GRAD}) \cdot VO)$$
$$= \frac{E1\,NO\,Q}{M} + \frac{EO\,N1\,Q}{M} - N1\,(D_T \cdot VO) + \frac{N1\,Q\,(VO \cdot (\mathrm{XPDT} \cdot BO))}{M} + \frac{NO\,Q\,(VO \cdot (\mathrm{XPDT} \cdot B1))}{M} - N1\,((VO \cdot \mathrm{GRAD}) \cdot VO)$$
$$- (\mathrm{GRAD} \cdot N1)\,\mathrm{VTH}^2$$

(E13) $$\mathrm{GRAD} \cdot (N1 \cdot VO) + D_T \cdot N1 = -\,\mathrm{GRAD} \cdot (NO \cdot V1)$$

(E14) $$NO\,(D_T \cdot V2) + NO\,((VO \cdot \mathrm{GRAD}) \cdot V2) - \frac{NO\,Q\,(V2 \cdot (\mathrm{XPDT} \cdot BO))}{M} + NO\,((V2 \cdot \mathrm{GRAD}) \cdot VO)$$
$$= \frac{E2\,NO\,Q}{M} + \frac{E1\,N1\,Q}{M} + \frac{EO\,N2\,Q}{M} - N2\,(D_T \cdot VO) - N1\,(D_T \cdot V1) + \frac{N2\,Q\,(VO \cdot (\mathrm{XPDT} \cdot BO))}{M} + \frac{N1\,Q\,(VO \cdot (\mathrm{XPDT} \cdot B1))}{M}$$
$$+ \frac{NO\,Q\,(VO \cdot (\mathrm{XPDT} \cdot B2))}{M} - N2\,((VO \cdot \mathrm{GRAD}) \cdot VO) - N1\,((VO \cdot \mathrm{GRAD}) \cdot V1) + \frac{N1\,Q\,(V1 \cdot (\mathrm{XPDT} \cdot BO))}{M}$$
$$+ \frac{NO\,Q\,(V1 \cdot (\mathrm{XPDT} \cdot B1))}{M} - N1\,((V1 \cdot \mathrm{GRAD}) \cdot VO) - NO\,((V1 \cdot \mathrm{GRAD}) \cdot V1) - (\mathrm{GRAD} \cdot N2)\,\mathrm{VTH}^2$$

(E15) $$\mathrm{GRAD} \cdot (N2 \cdot VO) + D_T \cdot N2 = -\,\mathrm{GRAD} \cdot (NO \cdot V2) - \mathrm{GRAD} \cdot (N1 \cdot V1)$$

(E16) $$NO\,(D_T \cdot V3) + NO\,((VO \cdot \mathrm{GRAD}) \cdot V3) - \frac{NO\,Q\,(V3 \cdot (\mathrm{XPDT} \cdot BO))}{M} + NO\,((V3 \cdot \mathrm{GRAD}) \cdot VO)$$
$$= \frac{E3\,NO\,Q}{M} + \frac{E2\,N1\,Q}{M} + \frac{E1\,N2\,Q}{M} + \frac{EO\,N3\,Q}{M} - N3\,(D_T \cdot VO) - N2\,(D_T \cdot V1) - N1\,(D_T \cdot V2) + \frac{N3\,Q\,(VO \cdot (\mathrm{XPDT} \cdot BO))}{M}$$
$$+ \frac{N2\,Q\,(VO \cdot (\mathrm{XPDT} \cdot B1))}{M} + \frac{N1\,Q\,(VO \cdot (\mathrm{XPDT} \cdot B2))}{M} + \frac{NO\,Q\,(VO \cdot (\mathrm{XPDT} \cdot B3))}{M} - N3\,((VO \cdot \mathrm{GRAD}) \cdot VO)$$
$$- N2\,((VO \cdot \mathrm{GRAD}) \cdot V1) - N1\,((VO \cdot \mathrm{GRAD}) \cdot V2) + \frac{N2\,Q\,(V1 \cdot (\mathrm{XPDT} \cdot BO))}{M} + \frac{N1\,Q\,(V1 \cdot (\mathrm{XPDT} \cdot B1))}{M}$$
$$+ \frac{NO\,Q\,(V1 \cdot (\mathrm{XPDT} \cdot B2))}{M} - N2\,((V1 \cdot \mathrm{GRAD}) \cdot VO) - N1\,((V1 \cdot \mathrm{GRAD}) \cdot V1) - NO\,((V1 \cdot \mathrm{GRAD}) \cdot V2)$$
$$+ \frac{N1\,Q\,(V2 \cdot (\mathrm{XPDT} \cdot BO))}{M} + \frac{NO\,Q\,(V2 \cdot (\mathrm{XPDT} \cdot B1))}{M} - N1\,((V2 \cdot \mathrm{GRAD}) \cdot VO) - NO\,((V2 \cdot \mathrm{GRAD}) \cdot V1) - (\mathrm{GRAD} \cdot N3)\,\mathrm{VTH}^2$$

(E17) $$\mathrm{GRAD} \cdot (N3 \cdot VO) + D_T \cdot N3 = -\,\mathrm{GRAD} \cdot (NO \cdot V3) - \mathrm{GRAD} \cdot (N1 \cdot V2) - \mathrm{GRAD} \cdot (N2 \cdot V1)$$

(D17) [E10, E11, E12, E13, E14, E15, E16, E17]

Fig. VI-6. Expansion of vector differential equations using the EXPEQS function.

significance of the EXPEQS function is the generality of expressions it is capable of handling. Among these are expressions involving any linear or bilinear operator, such as derivatives, integrals, or functions declared linear, and the dot operator "." and any operator defined in terms of it. This means that single variables may represent vectors, matrices, or tensors, which is the way expansions are generally done by hand. The restructuring of the expanded equations is a useful feature not commonly available elsewhere. By using the pattern-matching facility, the generality of this function can easily be extended by declaring how special functions or forms should be expanded. Examples of the EXPEQS function are given in Fig. VI-6. This function is limited to equations that are only algebraically nonlinear (variables to be expanded are raised only to integer powers) or which have special expansions declared by pattern matching. It should be pointed out that the process of expanding often results in apparent side effects, such as causing factored expressions to become expanded and pulling scalars out of vector products. MACSYMA's Taylor's series facility is useful for expanding other types of nonlinearities (i.e., transcendental) but even this is not sufficient for terms like $\frac{\overline{\nabla} n^{\gamma}(\bar{r}, t)}{n(\bar{r}, t)}$, where a functional series expansion is needed. Consequently, a functional expansion program must know about operators such as $\overline{\nabla}$ and its relation to the function $n(\bar{r}, t)$.

```
Solve the zero order equation to eliminate D[t].VO :
(C18) EQ0:SOLVE(''(EQS[1]),D[T].VO);
```

$$(D18) \qquad D_T \cdot VO = \frac{EO\ NO\ Q + NO\ Q\ (VO \cdot (XPDT \cdot BO)) - M\ NO\ ((VO \cdot GRAD) \cdot VO) - (GRAD \cdot NO)\ M\ VTH^2}{M\ NO}$$

```
(C19) (MAKECONSTANT(VO,NO),EO:0,E2:0)$
Load rules for heuristically taking Fourier-Laplace transforms:
(C20) BATCH(RULES,VECDOT,DSK,BERS)$
(C20) (NOTCONST(XPRE):=IS(NOT(CONSTANT(XPRE))),
MATCHDECLARE(CONSTV,CONSTANT),
TELLSIMP(GRAD.ATRUE.BTRUE,ATRUE.GRAD.BTRUE+BTRUE.GRAD.ATRUE),
TELLSIMP(GRAD.CONSTV,0),
TELLSIMP((ATRUE.GRAD).CONSTV,0),
DEFRULE(XDT,D[T].ATRUE,%I*W*ATRUE),
DEFRULE(XDERV,'DIFF(ATRUE,T),%I*W*ATRUE),
DEFRULE(XGR,GRAD.ATRUE,-%I*K.ATRUE),
DEFRULE(XDZ,'DIFF(ATRUE,Z),-%I*K*ATRUE),
DEFRULE(XGR2,(BTRUE.GRAD).ATRUE,(BTRUE.(-%I*K)).ATRUE),
TRANSFORM(EXPR):=APPLY2(EXPR,XDT,XDERV,XGR,XDZ,XGR2))$
(C22) EQS[3],EVAL,DOTSCALRULES;
```

$$(D22) \quad -\frac{NO\ (V1 \cdot (XPDT \cdot BO))\ Q}{M} + NO\ (D_T \cdot V1) = \frac{N1\ (VO \cdot (XPDT \cdot BO))\ Q}{M} + \frac{NO\ (VO \cdot (XPDT \cdot B1))\ Q}{M} + \frac{NO\ E1\ Q}{M} - N1\ (D_T \cdot VO)$$

```
(C23) %,''(EQ0),EXPAND,DOTSCALRULES;
```

$$(D23) \quad -\frac{NO\ (V1 \cdot (XPDT \cdot BO))\ Q}{M} + NO\ (D_T \cdot V1) = \frac{NO\ (VO \cdot (XPDT \cdot B1))\ Q}{M} + \frac{NO\ E1\ Q}{M}$$

```
(C24) TRANSFORM(%);
```

$$(D24) \quad -\frac{NO\ (V1 \cdot (XPDT \cdot BO))\ Q}{M} + V1\ NO\ \%I\ W = \frac{NO\ (VO \cdot (XPDT \cdot B1))\ Q}{M} + \frac{NO\ E1\ Q}{M}$$

Fig. VI-7. Examples of Fourier-Laplace transforms by heuristic pattern matching.

A functional expansion program is closely tied in with the implementation of operators, and we are investigating both of these issues.

The second procedure in the derivation of a nonlinear current is to take Fourier-Laplace transforms. While an explicit integration capability for Laplace transforms exists in MACSYMA, this is clearly not the most practical approach, and heuristic pattern rules are more successfully employed. For linear equations this reduces trivially to substitutions such as $\frac{\partial}{\partial t} \rightarrow -i\omega$, $\overline{\nabla} \rightarrow i\bar{k}$. In the case of nonlinear equations, convolutions occur and pattern matching makes it easier to establish one's own conventions such as implied convolutions for forms like $\bar{v}_1^a n_1^b$ or $\bar{v}_1^a \times \bar{B}_1^b$. A recursive algorithm for transforming nonlinear expressions algebraically will be discussed in a subsequent report. An example of the linear case is given in Fig. VI-7.

The final step is to solve the transformed equations for the second-order current. This can be done by explicitly giving commands to MACSYMA to move terms in the equations to appropriate places and eliminating variables and equations. Our recent implementation of an inverse and exponential operator corresponding to the noncommutative (vector) product facilitates this procedure. More automated solution of vector equations requires the factoring of noncommutative products; this is now being implemented.

Techniques for Evaluation of Nonlinear Coupling Coefficients

The objective in evaluating nonlinear coupling coefficients for various cases of interest is to arrive at a simple model that will give growth rates and thresholds for the coupling, as well as a physical understanding of the coupling mechanism. This can be accomplished by tracing the effects of different nonlinearities and various approximations. Our previous evaluation scheme[1] was not found to be helpful, so new techniques have been tried and problem areas identified.

For an unmagnetized plasma, analytic results can be derived directly, by relying heavily on MACSYMA's interactive capabilities. In order to understand why interactive derivations encounter difficulties, consider the following environment. In MACSYMA there are two main ways in which expressions can be represented:

(i) general representation, which allows representation of any kind of expression; and

(ii) canonical rational representation, in which all expressions are put in a rational function form.

From the user's point of view, the general representation would almost always be the first choice, since an expression can generally be put in whatever form he wishes. It is very difficult, however, to implement powerful algorithms for simplification in this representation, whereas in the canonical rational form some desired operations, such as factoring, cancelation of common factors, taking greatest common divisors (GCD),

This example illustrates the undesirable side-effects of the rational function representation. factoring is carried out globally, locally and locally on all subexpressions.

(C7) `(X+Y)^2*(A+A*((A^3+3*A^2*B+3*A*B^2+B^3)*((X+Y)^2)))^-1;`

(D7)
$$\frac{(X+Y)^2}{A+A\,(A^3+3\,A^2\,B+3\,A\,B^2+B^3)\,(X+Y)^2}$$

Global factoring:

(C8) `FACTOR(%);`

(D8)
$$(X+Y)^2/(A\,(1+(A^3+3\,A^2\,B+3\,A\,B^2+B^3)\,X^2+(2\,A^3+6\,A^2\,B+6\,A\,B^2+2\,B^3)\,X\,Y + (A^3+3\,A^2\,B+3\,A\,B^2+B^3)\,Y^2))$$

Local factoring:

(C9) `SUBSTPART(FACTOR(PIECE),D7,2,2,2);`

(D9)
$$\frac{(X+Y)^2}{A+A\,(A+B)^3\,(X+Y)^2}$$

Local factoring of all subexpressions:
(factorin is a user defined function)

(C10) `FACTORIN(D7);`

(D10)
$$\frac{(X+Y)^2}{A\,(1+(A+B)^3\,X^2+2\,(A+B)^3\,X\,Y+(A+B)^3\,Y^2)}$$

Use of the MULTTHRU command for carrying out simple manipulations:

Display the definition of a user function for pullling-out expressions from a sum:

(C13) `DISPFUN(PULLOUT);`

(D13) `PULLOUT(X, Y) := BLOCK([], IF PART(Y, 0) = "*" THEN Y : MULTTHRU(Y) ELSE FALSE,`

`IF NOT (PART(Y, 0) = "+") THEN RETURN(Y) ELSE FALSE, RETURN(MULTTHRU(1/X, Y) X))`

Local application of the PULLOUT function:

(C14) `SUBSTPART(PULLOUT(A,PIECE),D9,2);`

(D14)
$$\frac{(X+Y)^2}{A\,(1+(A+B)^3\,(X+Y)^2)}$$

Cross multiplication by XTHRU as compared to forming the expression over a common denominator using RATSIMP:

(C15) `(X+Y)^2/(A+B)^3+(E+F)^5/(Z+W)^2;`

(D15)
$$\frac{(X+Y)^2}{(A+B)^3}+\frac{(E+F)^5}{(W+Z)^2}$$

(C16) `RATSIMP(%);`

(D16)
$$(A^3\,(E^5+5\,E^4\,F+10\,E^3\,F^2+10\,E^2\,F^3+5\,E\,F^4+F^5) + B^3\,(E^5+5\,E^4\,F+10\,E^3\,F^2+10\,E^2\,F^3+5\,E\,F^4+F^5)+A^2\,B\,(3\,E^5+15\,E^4\,F+30\,E^3\,F^2+30\,E^2\,F^3 + 15\,E\,F^4+3\,F^5)+A\,B^2\,(3\,E^5+15\,E^4\,F+30\,E^3\,F^2+30\,E^2\,F^3+15\,E\,F^4+3\,F^5) + X^2\,(W^2+2\,W\,Z+Z^2)+Y^2\,(W^2+2\,W\,Z+Z^2)+X\,Y\,(2\,W^2+4\,W\,Z+2\,Z^2))/(A^3\,(W^2+2\,W\,Z+Z^2)+B^3\,(W^2+2\,W\,Z+Z^2)+A^2\,B\,(3\,W^2+6\,W\,Z+3\,Z^2) + A\,B^2\,(3\,W^2+6\,W\,Z+3\,Z^2))$$

(C17) `FACTOR(%);`

(D17)
$$(A^3\,(E^5+5\,E^4\,F+10\,E^3\,F^2+10\,E^2\,F^3+5\,E\,F^4+F^5) + B^3\,(E^5+5\,E^4\,F+10\,E^3\,F^2+10\,E^2\,F^3+5\,E\,F^4+F^5)+A^2\,B\,(3\,E^5+15\,E^4\,F+30\,E^3\,F^2+30\,E^2\,F^3 + 15\,E\,F^4+3\,F^5)+A\,B^2\,(3\,E^5+15\,E^4\,F+30\,E^3\,F^2+30\,E^2\,F^3+15\,E\,F^4+3\,F^5) + X^2\,(W^2+2\,W\,Z+Z^2)+Y^2\,(W^2+2\,W\,Z+Z^2)+X\,Y\,(2\,W^2+4\,W\,Z+2\,Z^2))/((A+B)^3\,(W+Z)^2)$$

Simple cross-multiply:

(C18) `XTHRU(D15);`

(D18)
$$\frac{(A+B)^3\,(E+F)^5+(X+Y)^2\,(W+Z)^2}{(A+B)^3\,(W+Z)^2}$$

Fig. VI-8. Examples of factoring techniques.

and general simplification, can be carried out very efficiently and quickly. The negative side effect of operations in rational form is that expressions are always put in the standard ratio-of-polynomials form (hence expanded somewhat), which may thwart the user in his attempt to format his results in an understandable form. The problem is, then, to reconcile these two forms. Several techniques are available. First, a partially factored representation is being developed which always refactors the results of rational operation and keeps previously factored subexpressions intact. This should substantially reduce the size of expressions that undergo rational operations such as GCDs, a major problem in our previous attempts at directly evaluating coupling coeffecients. A second technique is to apply only rational operations locally in an expression. The SUBSTPART command is available for this purpose. Figure VI-8 illustrates the difference between factoring locally, using SUBSTPART, and factoring globally. Commands such as MULTTHRU and XTHRU, which work in the general representation, allow such simple local operations as multiplying through or cross-multiplying, without removing the structure of subexpressions. These functions are also illustrated in Fig. VI-8.

Another useful technique is to put into an expression dummy undefined functions which the simplifier (the program which carries out simplification) will not remove. This dummy function may be transparent, or may have the special display property of putting a box around its argument and, in addition, it may be given a label when used as a box; all of these features help the user to keep track of important subexpressions. These techniques are illustrated in Fig. VI-9. The boxing function is also useful for identifying subexpressions interactively, so that the user can communicate to MACSYMA which part of an expression he is referring to. This is similar to a light pen facility in other systems.

a. Coupling Coefficients for an Unmagnetized Plasma

Now consider the derivation of a nonlinear coupling coefficient for an unmagnetized plasma, starting with an expression for the nonlinear current such as Eq. 19 in our previous report.[1] Figure VI-10 gives the actual computer output for the derivation. (The lines labeled C_i are Command lines typed by the user, while the D_i lines are the Display lines returned by MACSYMA.) The first step is to load in various previously defined rules, functions, expressions, and parameters that are useful for this derivation. The rules are typically pattern replacements such as the following.

$$\bar{E}_a \rightarrow \frac{|\bar{E}_a|}{|\bar{k}_a|}\,\bar{k}_a \qquad \text{(electrostatic approximation)}$$

$$\bar{E}_a \cdot \bar{k}_a \text{ or } \bar{k}_a \cdot \bar{E}_a \rightarrow 0 \qquad \text{(electromagnetic assumption)}$$

```
Example of the box scheme for suppressing simplification:
(C2) TBOX(A/B)*TBOX(B/C)*TBOX(C/A);
                                       A   B   C
(D2)                                  (-) (-) (-)
                                       B   C   A

(C3) SEEBOX(%);
                                      *** *** ***
                                      *A* *B* *C*
(D3)                                  *-* *-* *-*
                                      *B* *C* *A*
                                      *** *** ***

(C4) TOFFBOX(%);
                                       A   B   C
(D4)                                  (-) (-) (-)
                                       B   C   A
(C5) REMBOX(%);
(D5)                                        1
(C6) (X+Y)^2-TBOX((X+Y)^2);
                                       2            2
(D6)                           (X + Y)  - ((X + Y) )
(C7) REMBOX(%);
(D7)                                        0
Example of using boxes to keep track of important subexpressions and labeling them:

(C10) E[N].LBOX(SIGMA[N].E[N],CURRENT);
                                         *CURRENT*****
(D10)                              E  . *SIGMA  . E *
                                    N    *     N    N*
                                         *************
(C11) TOFFBOX(%);
(D11)                              E  . (SIGMA  . E )
                                    N          N   N
Example of simplification suppression for formating results:

(C12) -(SQRT(W[BG])*SQRT(W[IA])*SQRT(W[O])*QE)
/2/SQRT(2)/SQRT(MI)/SQRT(ME)/SQRT(EP[O])/W[PE]/C[S];

                         SQRT(W  ) SQRT(W  ) SQRT(W ) QE
                               BG        IA        O
(D12)              - -------------------------------------------
                     2 SQRT(2) SQRT(ME) SQRT(MI) SQRT(EP ) W   C
                                                        O   PE  S

(C13) TBOX(QE/ME)*TBOX(ME/MI)^TBOX(1/2)*TBOX(W[BG]*W[IA]*W[O])^TBOX(1/2)/4/S
QRT(2)/TBOX(EP[O]/4)^TBOX(1/2)/C[S];

                        ME (1/2)              (1/2)  QE
                       (--)      (W   W   W )       (--)
                        MI         BG  IA  O         ME
(D13)                  -------------------------------------
                                     EP
                                       O (1/2)
                           4 SQRT(2) (--)       C
                                      4          S
```

Fig. VI-9. Use of boxes in simplification suppression, labeling, and formating.

$$\bar{k}_a \cdot \bar{k}_b \rightarrow |\bar{k}_a||\bar{k}_b| \cos\theta_{ab} \qquad \text{(cosine form of dot product)}$$

A special factoring function is loaded which allows all subexpressions to be factored automatically. Finally, a file containing the general form of the coupling coefficient is loaded. Next we declare $\bar{E}$ and $\bar{k}$ to be nonscalar objects. Normally, we would also declare $\bar{\bar{\sigma}}$ to be nonscalar, but for the unmagnetized plasma case this is not necessary because σ is a scalar.

Next the general expression is displayed for the coupling coefficient, specialized to the ion species. Note that we have dropped the continuity and pressure nonlinear terms under the assumption of a cold-plasma model for the ions. First, we put labeled boxes on important subexpressions to illustrate this capability, and then remove them at the next step. In order to simplify the expression under the assumption of a scalar σ, we invoke vector simplification rules with the flag DOTSCALRULES. The effect is to make transformationlike M1 . (S*M2) → S* (M1 . M2), where M1 and M2 are nonscalar expressions, and S is a scalar expression. Next we introduce the electrostatic assumption,

$$\bar{E}_a \rightarrow \frac{|\bar{E}_a|}{|\bar{k}_a|}\,\bar{k},$$

noting that the Lorentz term reduces to zero as expected. Then the expression is factored. We have not lost much in the way of the structure of the result because of the imposed boxes and transparent boxes about terms like $\left(-\frac{i}{2\omega_n n_o \epsilon_o \omega_{pi}^2 q_i}\right)$. By using the resonance condition $\bar{k}_n = \bar{k}_a + \bar{k}_b$, the result can be simplified further. From this point, the contributions from the CONVEC (convective) and FLOWCUR (flow current) nonlinearities can easily be identified, so the boxes can be removed. The expression for the ion term is then put in final form by defining σ, factoring, and multiplying-through to get the desired form. Forms in terms of angles between the wavevectors or for the collinear case are then given.

Similar steps are taken for the electron term, and we can now evaluate the results for ions and electrons for some particular case. Consider the familiar coupling between two Bohm-Gross waves and an ion acoustic wave. Let

$$\omega_n \rightarrow \omega_{1A} \quad \text{and} \quad \frac{k_{1A}}{\omega_{1A}} = \frac{1}{c_S}; \qquad \frac{k_{BG1}}{\omega_{BG1}} \cong 0;$$

$$\omega_a \rightarrow \omega_{BG1} \cong \omega_{PE}; \qquad \omega_b \rightarrow \omega_{BG2}; \qquad \frac{k_{BG2}}{\omega_{BG2}} = \frac{1}{v_{BG2}} \ll \frac{1}{c_S}.$$

This result is shown in Fig. VI-11.

```
This is an example of a straightforward derivation using an unmagnetized plasma model.
First, general expressions are derived for each species (ions and electrons) in the
appropriate limits of interest: unmagnetized cold plasma model for the ions; collinear,
warm plasma model for the electrons.  Then the expressions are specialized for the
coupling of a pump wave with zero wavenumber to a Bohm-Gross wave and an ion acoustic
wave.  Finally expressions for the energy of these waves and the growth rate of the single
pump case are calculated.

Load in the preliminaries:

(C4) BATCH([UNMAG,?>,DSK,PLASMA],ON);

(C4) (LOADFILE(UNMAG,LRULES,DSK,PLASMA),LOADFILE(LFUNS,FACTOR,DSK,BERS), LOADFILE(CCSIG,SAVE,DSK,PLASMA),MAXAPPLYDEPTH:
20,
?MPUTPROP(E,?CDR([NONSCALAR]),?ARRAYPROPS),?MPUTPROP(K,?CDR([NONSCALAR]),?ARRAYPROPS),?MPUTPROP(?MNCTIMES,?CDR([SCALAR]
),?FUNCPROPS))$

UNMAG LRULES DSK PLASMA BEING LOADED
LOADING DONE

LFUNS FACTOR DSK BERS BEING LOADED
LOADING DONE

CCSIG SAVE DSK PLASMA BEING LOADED
LOADING DONE

(C5) /*
CALCULATE ION TERM
*/
The general expression for the coupling coefficent for a fluid model:

EJTOTI:EV(LBOX(CCEMJXB(N,A,B),LORENTZ)+LBOX(CCFLOWCUR(N,A,B),FLOWCUR)
+LBOX(CCCONVEC(N,A,B),CONVEC),P:PI,M:MI,Q:QI);

     *FLOWCUR******************************************************************************
     *                          *NB*****************  *NA*****************                 *
     *                          *K  . (SIGMA  . E )*  *K  . (SIGMA  . E )*                 *
     *         *VA*********** * B          B    B *  * A          A    A * *VB**********     1       *
(D5) *(E  . (*SIGMA  . E *  *------------------* + *------------------* *SIGMA  . E *)) (----------)*
     *  N      *     A   A* *        W          *  *        W          * *     B   B*   2 W  NO QI *
     *         ************ *         B         *  *         A         * ************     N        *
     *                          ********************  ********************                 *
     **************************************************************************************

      *LORENTZ********************************************************************************************
      *                          *VB**********                   *VB**********                    *VA**********
      *               K  (E  . *SIGMA  . E *)          E  (K  . *SIGMA  . E *)          K  (E  . *SIGMA  . E *)
      *                A   A   *     B   B*             A   A   *     B   B*             B   B   *     A   A*
      *                        ************                     ************                     ************
    + *(E  . (SIGMA  . ------------------------- - SIGMA  . ------------------------- + SIGMA  . -------------------------
      *  N         N               W                    N               W                    N               W
      *                             A                                    A                                    B
      ****************************************************************************************************

     ************************************************************
     *                       *VA**********                       *
     *             E  (K  . *SIGMA  . E *)                       *
     *              B   B   *     A   A*                         *
     *                      ************            1            *
    - SIGMA  . ----------------------------)) (------------)*
     *      N               W                   2 W  NO QI  *
     *                       B                     N        *
     ************************************************************

      *CONVEC****************************************************************************************
      *               *VA**********     *VB**********             *VA**********   *VB**********
    + *(E  . (SIGMA  . (*SIGMA  . E * . K ) *SIGMA  . E * + SIGMA  . *SIGMA  . E * (*SIGMA  . E * . K )))
      *  N         N   *     A   A*    B  *     B   B*         N  *     A   A*   *     B   B*    A
      *               ************      ************              ************    ************
      *
      ***********************************************************************************************

     **************************
     (  -        %I           )*
          -----------------    *
                       2       *
          2 W  NO EP  W     QI *
             N      O  PI      *
     **************************

Restructure the expression under the assumption that SIGMA is a scalar:

(C6) EJTOTI:EV(TOFFBOX(EJTOTI),DOTSCALRULES);

                SIGMA  (K  . E )                                  SIGMA  (K  . E )
                     A   A    A                                        B   B    B               1
(D6) ((E  . ((----------------) (E  SIGMA ) + (E  SIGMA ) (----------------))) (----------))
        N             W            B      B      A      A          W                 2 W  NO QI
                       A                                            B                   N

              K  (E  . (E  SIGMA )) SIGMA     E  (K  . (E  SIGMA )) SIGMA     K  (E  . (E  SIGMA )) SIGMA
               A   A     B      B        N     A   A     B      B        N     B   B     A      A
    + ((E  . (------------------------------ - ------------------------------ + ------------------------------
         N                 W                               W                               W
                            A                               A                               B

      E  (K  . (E  SIGMA )) SIGMA
  N    B   B     A      A        N           1
  - - ------------------------------)) (----------))
                  W                      2 W  NO QI
                   B                        N

                                                                                                        %I
    + ((E  . (((E  SIGMA ) . K ) (E  SIGMA ) SIGMA  + (E  SIGMA ) ((E  SIGMA ) . K ) SIGMA )) ( - -------------------))
         N      A      A      B    B      B       N     A      A     B      B      A       N                         2
                                                                                                 2 W  NO EP  W     QI
                                                                                                    N      O  PI
```

Fig. VI-10. Derivation of the coupling coefficient for an unmagnetized plasma.

The electrostatic assumption (for plasma waves and ion acoustic waves):

(C7) DISPRULE(ELSTAT);

(D7)
$$E_{ATRUE} = \frac{K_{ATRUE}\,E_{ATRUE}}{K_{ATRUE}}$$

(C8) EJTOTI:ELECTSTAT(EJTOTI);

(D8)
$$\left(\left(\frac{K_N E_N}{K_N}\right)\cdot\left(\left(\frac{\mathrm{SIGMA}_A\left(K_A - \frac{K_A E_A}{K_A}\right)}{W_A}\right)\left(\frac{K_B \mathrm{SIGMA}_B E_B}{K_B}\right) + \left(\frac{K_A \mathrm{SIGMA}_A E_A}{K_A}\right)\left(\frac{\mathrm{SIGMA}_B\left(K_B - \frac{K_B E_B}{K_B}\right)}{W_B}\right)\right)\left(\frac{1}{2\,W_N\,NO\,QI}\right)\right)$$

$$+\left(\left(\frac{K_N E_N}{K_N}\right)\cdot\left(-\frac{K_A E_A\left(K_A - \left(\frac{K_B \mathrm{SIGMA}_B E_B}{K_B}\right)\right)\mathrm{SIGMA}_N}{W_A K_A} + \frac{K_A\left(\frac{K_A E_A}{K_A} - \left(\frac{K_B \mathrm{SIGMA}_B E_B}{K_B}\right)\right)\mathrm{SIGMA}_N}{W_A}\right)\right.$$

$$\left.-\frac{N\,K_B E_B\left(K_B - \left(\frac{K_A \mathrm{SIGMA}_A E_A}{K_A}\right)\right)\mathrm{SIGMA}_N}{W_B K_B} + \frac{K_B\left(\frac{K_B E_B}{K_B} - \left(\frac{K_A \mathrm{SIGMA}_A E_A}{K_A}\right)\right)\mathrm{SIGMA}_N}{W_B}\right)\left(\frac{1}{2\,W_N\,NO\,QI}\right)\right)$$

$$+\left(\left(\frac{K_N E_N}{K_N}\right)\cdot\left(\left(\frac{K_A \mathrm{SIGMA}_A E_A}{K_A}\right)\cdot K_B\right)\left(\frac{K_B \mathrm{SIGMA}_B E_B}{K_B}\right)\mathrm{SIGMA}_N + \left(\frac{K_A \mathrm{SIGMA}_A E_A}{K_A}\right)\left(\left(\frac{K_B \mathrm{SIGMA}_B E_B}{K_B}\right)\cdot K_A\right)\mathrm{SIGMA}_N\right)$$

$$\left)\left(-\frac{\%I}{2\,W_N\,NO\,EP_O\,W_{PI}^{\,2}\,QI}\right)\right)$$

(C9) EJTOTI:EV(''REMBOX(EJTOTI,LORENTZ,VA,VB,NA,NB),EXPAND,DOTSCALRULES)$

(C10) EJTOTI:SEEBOX(''FACTORIN(EJTOTI),LBOXES);

(D10)
$$\frac{\mathrm{SIGMA}_A E_A\ \mathrm{SIGMA}_B E_B\ E_N\left(W_A K_A^{\,2}\left(K_N - K_A\right) + K_A W_B^{\,2}\left(K_N - K_B\right)\right)\left(\frac{1}{2\,W_N\,NO\,QI}\right)}{W_A K_A W_B K_B K_N}$$

$$+\frac{\mathrm{SIGMA}_N\left(K_A - K_B\right)\left(K_A - K_N\right)\left(K_B - K_N\right)\left(-\frac{\%I}{2\,W_N\,NO\,EP_O\,W_{PI}^{\,2}\,QI}\right)}{K_A K_B K_N}$$

(C11) (DENOM1:PART(EJTOTI,1,1,2),DENOM2:PART(EJTOTI,2,1,2))$

(C12) EJTOTI:SUBSTPART(W[N]*DENOM2*LBOX((K[A]-K[B])*NORM(K[N])^2/W[N]/DENOM2,CONVEC),
REMBOX(EJTOTI,CONVEC),2,1,7)$

(C13) EJTOTI:SUBSTPART(DENOM1*LBOX(MULTTHRU(1/DENOM1,PIECE),FLOWCUR),
REMBOX(EJTOTI,FLOWCUR),1,1,6)$

The contributions due to the flow-current term and the convective term are identified.
Note the Lorentz force term has reduced to zero.

(C14) EJTOTI:FACTOR(REMBOX(SUBST(%I*EP[0]*W[PI]^2/W[N],SIGMA[N],EJTOTI),TBOXES));

(D14)
$$\frac{\mathrm{SIGMA}_A E_A\ \mathrm{SIGMA}_B E_B\ E_N\left(\frac{(K_A - K_B)K_N}{K_A K_B W_N} + \frac{K_B(K_N - K_A)}{K_A W_B K_N} + \frac{K_A(K_N - K_B)}{W_A K_B K_N}\right)}{2\,W_N\,NO\,QI}$$

(C15) SIGMA[I]:=%I*EP[0]*W[PI]^2/W[I];

(D15)
$$\mathrm{SIGMA}_I := \frac{\%I\,EP_O\,W_{PI}^{\,2}}{W_I}$$

The general expression for E.J/w for the ions:

(C16) EJTOTI:REMBOX(EJTOTI);

(D16)
$$\frac{\mathrm{SIGMA}_A E_A\ \mathrm{SIGMA}_B E_B\ E_N\left(\frac{(K_A - K_B)K_N}{K_A K_B W_N} + \frac{K_B(K_N - K_A)}{K_A W_B K_N} + \frac{K_A(K_N - K_B)}{W_A K_B K_N}\right)}{2\,W_N\,NO\,QI}$$

(C17) DOTRULE(EJTOTI);

(D17)
$$\frac{\mathrm{SIGMA}_A E_A\ \mathrm{SIGMA}_B E_B\ E_N\left(\frac{K_B\,\mathrm{COS}(\mathrm{ANGLE}_{KN,KA})}{W_B} + \frac{K_A\,\mathrm{COS}(\mathrm{ANGLE}_{KN,KB})}{W_A} + \frac{\mathrm{COS}(\mathrm{ANGLE}_{KA,KB})K_N}{W_N}\right)}{2\,W_N\,NO\,QI}$$

Collinear form:

(C18) EJTOTI:COS1RULE(%);

(D18)
$$\frac{\mathrm{SIGMA}_A E_A\ \mathrm{SIGMA}_B E_B\ E_N\left(\frac{K_A}{W_A} + \frac{K_B}{W_B} + \frac{K_N}{W_N}\right)}{2\,W_N\,NO\,QI}$$

(C19) EJTOTI:EV(EJTOTI,EVAL);

(D19)
$$-\frac{E_A E_B E_N\left(\frac{K_A}{W_A} + \frac{K_B}{W_B} + \frac{K_N}{W_N}\right)EP_O^{\,2}\,W_{PI}^{\,4}}{2\,W_A W_B W_N\,NO\,QI}$$

Fig. VI-10. (continued)

```
(C20) /*
CALCULATE ELECTRON TERM
*/

ELECTRONS&&
KILL(SIGMA,LABELS,E,K,?MNCTIMES,DOTRULE,ELECTSTAT,DENOM1,DENOM2,
    \^\^RULE1,ELSTAT,DOTCOS,COS1R1,COS1RULE)$

The general expression for E.J/w for the electrons:

(C2) LBOX(CCEMJXB(N,A,B),LORENTZ)+LBOX(CCFLOWCUR(N,A,B),FLOWCUR)
+LBOX(CCCONVEC(N,A,B),CONVEC)+LBOX(CCPRESSURE(N,A,B),PRESSURE)+
LBOX(CCCONTIN(N,A,B),CONTINUITY),P:PE,M:ME,Q:-QE;

     *FLOWCUR*************************************************************************
     *                    *NB*****************  *NA*****************                *
     *                    *K  . (SIGMA  . E )*  *K  . (SIGMA  . E )*                *
     *       *VA********** * B           B   B * * A           A   A * *VB**********      1      *
(D2) *(E  . (*SIGMA  . E * *------------------* + *------------------* *SIGMA  . E *)) ( - ----------)*
     *  N    *      A   A* *        W          * *        W          * *     B    B*     2 W  NO QE *
     *       ************* *         B         * *         A         * *************       N        *
     *                    ********************  ********************                *
     *********************************************************************************

       *LORENTZ*****************************************************************************************
       *                         *VB**********                    *VB**********                   *VA**********
       *               K  (E  . *SIGMA  . E *)          E  (K  . *SIGMA  . E *)         K  (E  . *SIGMA  . E *)
       *                A   A   *      B    B*           A   A   *      B    B*          B   B   *      A    A*
       *                        *************                    *************                  *************
     + *(E  . (SIGMA  . ---------------------------- - SIGMA  . ---------------------------- + SIGMA  . ---------------------
       *  N         N                W                      N                W                      N          W
       *                              A                                        A                                B
       ***************************************************************************************************

     ****************************************************
                  *VA**********                         *
          E  (K  . *SIGMA  . E *)                        *
           B   B   *      A    A*                        *
                  *************              1          *
     - SIGMA  . ------------------------)) ( - ----------)*
            N                W                2 W  NO QE *
                              B                  N       *
     ****************************************************


       *CONVEC*******************************************************************************
       *              *VA**********       *VB**********             *VA********** *VB**********
     + *(E  . (SIGMA  . (*SIGMA  . E * . K ) *SIGMA  . E * + SIGMA  . *SIGMA  . E * (*SIGMA  . E * . K )))
       *  N         N   *      A    A*     B *      B    B*        N *      A    A*  *      B    B*    A
       *                *************        *************          *************   *************
       *
       *************************************************************************************

                              *PRESSURE*****************************************************************
                              **NA****************** *NB*****************                       2     *
     ***********************  **K                  * *K                 *             %I G2V          *
     (          %I          )* + ** A                 * * B                *                   TH         *
     (----------------------)* + **-- . (SIGMA  . E )* *-- . (SIGMA  . E )* (E  . (SIGMA  . K )) (----------------------)*
     (                 2    )*   **W          A    A * *W          B    B * *  N         N    N  (                 2    )*
     2 W  NO EP  W      QE  *   ** A                 * * B                *             2 W  NO EP  W      QE *
        N      O   PE       *   ********************* ********************                N      O   PE      *
     ***********************  **************************************************************************

       *CONTINUITY*********************************************************************************
       *                 *NB*****************                           *NA*****************
       *                 *K                 *  K                        *K                 *  K
       *                 * B                *   N   *VA**********       * A                *   N   *VB**********
     + *(E  . (SIGMA  . K ) (*-- . (SIGMA  . E )* (-- . *SIGMA  . E *) + *-- . (SIGMA  . E )* (-- . *SIGMA  . E *)))
       *  N         N    N   *W          B    B *  W    *      A    A*     *W          A    A *  W    *      B    B*
       *                 * B                *   N   *************      * A                *   N   *************
       *                 ********************                          ********************
       *********************************************************************************************

     ***********************
                   2       *
           %I GV           *
                 TH        *
     (----------------------)*
                       2   *
     2 W  NO EP  W      QE *
        N      O   PE      *
     ***********************

Specialize to the collinear electrostatic case:

(C3) EJTOTE:NORM(E[A])*NORM(E[B])*NORM(E[N])*EV(''(TOFFBOX(REMBOX(%,LORENTZ,VA,VB,NA,NB))/K[A]/K[B]/K[N]),E=K,\.=\*,
EXPAND)$

(C4) SIGMA[I]:=EP[O]*W[PE]^2*%I*W[I]/(W[I]^2-V[TH,E]^2*K[I]^2);

                                                             2
                                              %I W  EP  W
                                                  I   O   PE
(D4)                                 SIGMA  := -----------------
                                          I      2    2       2
                                                W  - K  V
                                                 I    I  TH, E

(C5) KILL(CCEMJXB,CCFLOWCUR,CCCONVEC,CCPRESSURE,CCCONTIN)$
```

Fig. VI-10. (continued)

(C6) EJTOTE:EV(SEEBOX(EJTOTE,LBOXES),EVAL);

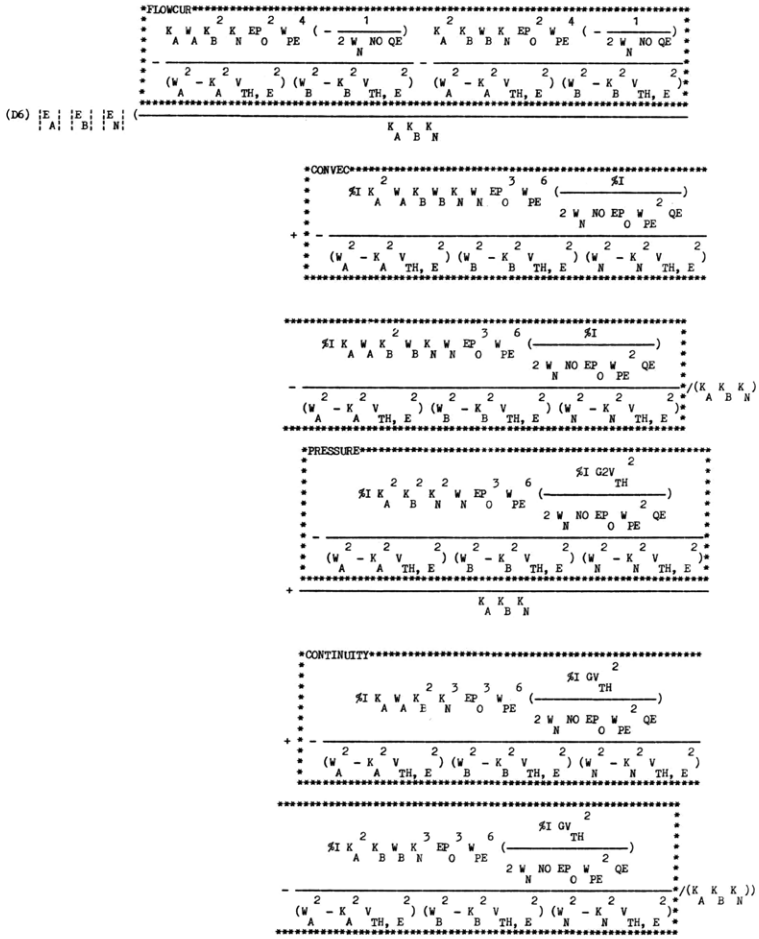

(C7) DEFRULE(MANIP,W[ATRUE]^2-K[ATRUE]^2*V[TH,E]^2,W[ATRUE]^2*F[ATRUE])$

MATCOM FASL DSK MACSYM BEING LOADED
LOADING DONE

(C8) EJTOTE:FACTOR(APPLY1(SUBST([?MLABOX=*,?TBOX=*],EJTOTE),MANIP))$

(C9) F[I]:=1-K[I]^2*V[TH,E]^2/W[I]^2$

(C10) EJTOTE:EV(EJTOTE,EVAL)$

This expression allows identification of the origin of various terms, necessary for determining the physical mechanism&

(C11) SUBSTPART(W[A]*W[B]*W[N]^2*EXPAND(RATSIMP(PIECE/W[A]/W[B]/W[N]^2)),
EJTOTE,1,6);

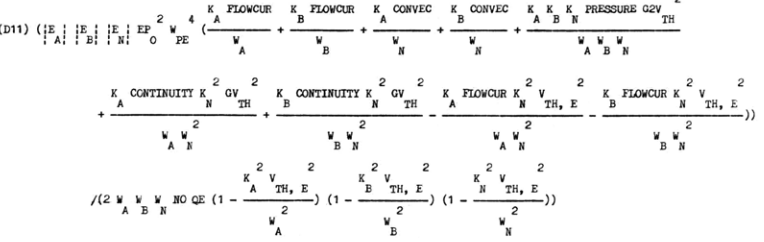

(C12) EJTOTE:EV(''%,GV[TH]^2=V[TH,E]^2,G2V[TH]^2=V[TH,E]^2,FLOWCUR=1,CONVEC=1,CONTINUITY=1,PRESSURE=1)$

The final expression for E.J/w for the electrons:

(C13) EJTOTE:SUBSTPART(K[N]/W[N],EJTOTE,1,6,[3,4]);

(D13)

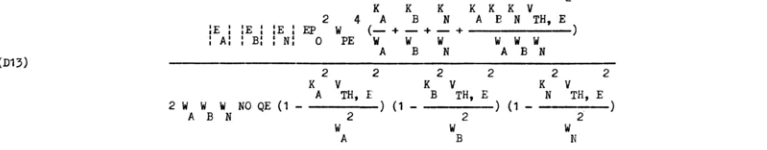

Fig. VI-10. (concluded)

```
(C14) /*
CALCULATE DENOMINATOR OF COUPLING COEFF.
*/

CC&&

Calculation of the energies; the dispersion function:

DISPFN:1-W[PI]^2/W[I]^2-W[PE]^2/(W[I]^2-K[I]^2*V[TH,E]^2);
```

$$(D14)\qquad 1-\frac{W_{PI}^2}{W_I^2}-\frac{W_{PE}^2}{W_I^2-K_I^2V_{TH,E}^2}$$

```
(C15) DN:EV(''DIFF(DISPFN,W[I]),I=N);
```

$$(D15)\qquad \frac{2W_{PI}^2}{W_N^3}+\frac{2W_N^2W_{PE}^2}{(W_N^2-K_N^2V_{TH,E}^2)^2}$$

```
(C16) 2*W[PE]^2/W[N]^3*MULTTHRU(W[N]^3/2/W[PE]^2,SUBSTPART(W[N]^2*EXPAND(PIECE/W[N]^2),DN,2,2,1));
```

$$(D16)\qquad \frac{2W_{PE}^2\left(\frac{W_{PI}^2}{W_{PE}^2}+\frac{1}{\left(1-\frac{K_N^2V_{TH,E}^2}{W_N^2}\right)^2}\right)}{W_N^3}$$

```
(C17) (DWO:2*W[PE]^2/W[O]^3,DBG:2*W[BG]/W[PE]^2,DIA:2*W[PI]^2/W[IA]^3);
```

$$(D17)\qquad \left[\frac{2W_{PE}^2}{W_O^3},\frac{2W_{BG}}{W_{PE}^2},\frac{2W_{PI}^2}{W_{IA}^3}\right]$$

```
(C18) D:DWO*DBG*DIA;
```

$$(D18)\qquad \frac{8W_{BG}W_{PI}^2}{W_{IA}^3W_O^3}$$

```
(C19) TELLSIMP(NORM(K[ATRUE]),K[ATRUE])$
RULE PLACED ON NORM

(C20) (EJTOTI:EV(EJTOTI,SIMP),NORMS:NORM(E[A])*NORM(E[B])*NORM(E[N]))$

The expression for the full normalized coupling coefficient, identifying the ion and electron contributions:
Specialized to the Bohm-Gross coupling problem.

(C21) CC:EV(''(LBOX(EJTOTI/NORMS,IONS)+LBOX(EJTOTE/NORMS,ELECTRONS))/D^(1/2)/(EP[O]/4)^(3/2)/4,
QI=QE,W[N]=W[IA],W[A]=W[O],W[B]=-W[BG],K[A]=0,
K[N]=W[IA]/C[S], K[B]= W[BG]/V[BG]);
```

$$(D21)\qquad \frac{W_{IA}^{3/2}W_O^{3/2}\left(\frac{2W_{BG}W_{IA}W_{NO}W_{QE}}{W_O}\right)+\left(-\frac{2W_{BG}^2W_{PE}^2\left(-\frac{1}{V_{BG}^2}+\frac{1}{C_S^2}\right)}{W_O^2}\right)\left(1-\frac{1}{V_{TH,E}^2}\right)^2\left(1-\frac{1}{V_{TH,E}^2}\right)^2}{\sqrt{2}\sqrt{W_{BG}}EP_O^{3/2}W_{PI}}$$

Fig. VI-11. Specialization to the Bohm-Gross problem.

Use physical approximations like V[BG] >> C[S], V[TH,E]^2/C[S]^2 = MI/ME :

```
(C22) CC:EV(''CC,?MIABOX=\*,W[PI]=W[PE]*SQRT(ME/MI),W[PI]^4=W[PE]^2*(QE^2*NO/ME/EP[O])*ME^2/MI^2,
W[PE]=(QE^2*NO/ME/EP[O])^(1/2),(1-V[TH,E]^2/C[S]^2)=MI/ME, (1-V[TH,E]^2/V[BG]^2)=W[PE]^2/W[BG]^2,1/V[BG]=0);
```

$$(D22)\qquad \frac{W_{IA}^{3/2}\,\mathrm{SQRT}(MI)\,W_{O}^{3/2}\left(-\frac{W_{BG}\,\mathrm{ELECTRONS}\,EP_{O}\,QE}{2\,W_{IA}\,MI\,W_{O}\,C_{S}}+\frac{\mathrm{IONS}\,EP_{O}\,W_{PE}^{2}\,QE}{2\,W_{BG}\,W_{IA}\,MI\,W_{O}\,C_{S}}\,MR\right)}{\mathrm{SQRT}(2)\,\mathrm{SQRT}(W_{BG})\,\mathrm{SQRT}(ME)\,EP_{O}^{3/2}\,W_{PE}}$$

Final expression for the coupling coefficient:

```
(C23) CC:EV(CC,IONS=0,ELECTRONS=1);
```

$$(D23)\qquad -\frac{\mathrm{SQRT}(W_{BG})\,\mathrm{SQRT}(W_{IA})\,\mathrm{SQRT}(W_{O})\,QE}{2\,\mathrm{SQRT}(2)\,\mathrm{SQRT}(ME)\,\mathrm{SQRT}(MI)\,\mathrm{SQRT}(EP_{O})\,W_{PE}\,C_{S}}$$

Final expression formated:

```
(C24) TBOX(QE/ME)*SQRT(TBOX(W[BG]*W[IA]*W[O]))*SQRT(TBOX(ME/MI))/SQRT(2)/4/C[S]/SQRT(TBOX(EP[O]/4));
```

$$(D24)\qquad \frac{\mathrm{SQRT}\left(\frac{ME}{MI}\right)\mathrm{SQRT}\left(W_{BG}\,W_{IA}\,W_{O}\right)\left(\frac{QE}{ME}\right)}{4\,\mathrm{SQRT}(2)\,\mathrm{SQRT}\left(\frac{EP_{O}}{4}\right)C_{S}}$$

Calculate the growth rate of the pump from the coupling coefficient:

```
(C25) GROWTH\-RATE=EV(-CC*(W[O]*ME*V[O]/QE)*SQRT(DWO*EP[O]/4),C[S]=V[TH,E]*SQRT(ME/MI),W[PE]=SQRT(NO*QE^2/EP[O]/ME),
EVAL);
```

$$(D25)\qquad \mathrm{GROWTH\text{-}RATE} = \frac{\mathrm{SQRT}(W_{BG})\,\mathrm{SQRT}(W_{IA})\,V_{O}}{4\,V_{TH,\,E}}$$

Formated growth rate:

```
(C26) GROWTH\-RATE=SQRT(TBOX(W[BG]*W[IA]))*TBOX(V[O]/V[TH,E])/4;
```

$$(D26)\qquad \mathrm{GROWTH\text{-}RATE} = \frac{\mathrm{SQRT}\left(W_{BG}\,W_{IA}\right)\left(\frac{V_{O}}{V_{TH,\,E}}\right)}{4}$$

Fig. VI-11. (continued)

```
(C4) LOADFILE(SYMCC,NEW1,DSK,PLASMA)$
SYMCC NEW1 DSK PLASMA BEING LOADED
LOADING DONE
(C5) LOADFILE(LFCC,RFNS2,DSK,PLASMA)$
LFCC RFNS2 DSK PLASMA BEING LOADED
LOADING DONE
(C6) (KEEPFLOAT:TRUE,DOTNONASSOC:TRUE,NORAT:TRUE,FLOAT:TRUE,NOLABELS:TRUE)$
(C7) KILL(LABELS)$
Normalized form of the coupling coefficient which has been previously calculated:
(C2) CCELTOT:SUBST([AAA=A,BBB=B,NNN=N],EV(CCELTOT,REMBOX));
```

(D2)
$$\frac{0.5\, NE_A\, NE_B\, GM2\, (KN_N \cdot (\frac{SIGMAN_N}{CONSTSIG} \cdot KN_N))\, PRESSURE}{KNM_A\, KNM_B\, CONSTN^2\, MU\, KNM_N\, WN_N}$$

$$+ \frac{0.5\, FLOWCUR\, (\frac{NE_A\, (KN_N \cdot \frac{VE_B}{CONSTV})\, TERM1}{CONSTN} + \frac{NE_B\, (KN_N \cdot \frac{VE_A}{CONSTV})\, TERM2}{CONSTN})}{KNM_A\, KNM_B\, MU\, KNM_N\, WN_N}$$

$$+ (0.5\, CONVEC\, ((KN_B \cdot \frac{VE_A}{CONSTV})\, (KN_N \cdot (\frac{SIGMAN_N}{CONSTSIG} \cdot \frac{VE_B}{CONSTV}))\, TERM1 + (KN_A \cdot \frac{VE_B}{CONSTV})\, (KN_N \cdot (\frac{SIGMAN_N}{CONSTSIG} \cdot \frac{VE_A}{CONSTV}))$$

$$TERM2))/(KNM_A\, KNM_B\, MU^2\, KNM_N\, WN_N)$$

$$+ (0.5\, CONTIN\, (\frac{NE_A\, (KN_N \cdot \frac{VE_B}{CONSTV})\, (KN_N \cdot (\frac{SIGMAN_N}{CONSTSIG} \cdot \frac{KN_N}{WN_N}))\, TERM1}{CONSTN}$$

$$+ \frac{NE_B\, (KN_N \cdot \frac{VE_A}{CONSTV})\, (KN_N \cdot (\frac{SIGMAN_N}{CONSTSIG} \cdot \frac{KN_N}{WN_N}))\, TERM2}{CONSTN}))/(KNM_A\, KNM_B\, MU\, KNM_N\, WN_N)$$

```
(C3) CCIONTOT:SUBST([AAA=A,BBB=B,NNN=N],EV(CCIONTOT,REMBOX));
```

(D3)
$$- \frac{0.5\, FLOWCUR\, (\frac{NI_A\, (KN_N \cdot \frac{VI_B}{CONSTV})\, TERM1}{CONSTN} + \frac{NI_B\, (KN_N \cdot \frac{VI_A}{CONSTV})\, TERM2}{CONSTN})}{KNM_A\, KNM_B\, MU\, KNM_N\, WN_N}$$

$$- (0.5\, CONVEC\, ((KN_B \cdot \frac{VI_A}{CONSTV})\, (KN_N \cdot (\frac{SIGMAN_N}{CONSTSIG} \cdot \frac{VI_B}{CONSTV}))\, TERM1 + (KN_A \cdot \frac{VI_B}{CONSTV})\, (KN_N \cdot (\frac{SIGMAN_N}{CONSTSIG} \cdot \frac{VI_A}{CONSTV}))$$

$$TERM2))/(KNM_A\, KNM_B\, MU\, KNM_N\, WN_N)$$

```
(C4) CONSTFACT:SUBST([AAA=A,BBB=B,NNN=N],CONSTFACT);
```

(D4)
$$(\frac{E_A\, E_B\, E*_N\, EP_O\, WN_{PI}^2\, Q}{W_{CI}\, ME\, C_S}) .$$

```
(C5) NOTECASE;
(D5) IN THIS CASE WE EXPRESS THE COUPLING COEFF
IN TERMS OF V'S AND N'S.
TO GET E.J/W MULTIPLY CCELTOT+CCIONTOT BY CONSTFACT.  CONSTFACT
CARRIES ALL THE UNITS OF THE EXPRESSION, SO CCELTOT AND CCIONTOT
ARE DIMENSIONLESS.  THIS IS ACHIEVED BY INSERTING CONSTSIG, CONSTV
AND CONSTN IN THE EXPRESSIONS.  THEY ARE DEFINED AS FOLLOWS:
CONSTSIG:%I*EP[O]*W[CI]*WN[PI]^2,
CONSTV:CONSTSIG/NO/Q,  (NO=DENSITY, Q IS ABS(CHARGE)),
CONSTN:CONSTSIG/C[S]/Q.
Numerical quantities are read in and displayed.  Then velocities, densities, and the
coupling coefficient are calculated:
```

Fig. VI-12. Examples of seminumerical evaluation of the coupling coefficients and growth rates for estimates of important terms in the coupling of lower hybrid waves to ion acoustic waves.

```
(C25) BLOCK(VE[A]:-EV(SIGMAN[A].KN[A],EVAL,EXPAND,FLOAT),DISPLAY(VE[A]),
VE[B]:-EV(SIGMAN[B].KN[B],EVAL,EXPAND,FLOAT),DISPLAY(VE[B]),
NE[A]:EV(KN[A].(VE[A]/WN[A]),EVAL,EXPAND,FLOAT),DISPLAY(NE[A]),
NE[B]:EV(KN[B].(VE[B]/WN[B]),EVAL,EXPAND,FLOAT),DISPLAY(NE[B]),
DISPLAY(SIGMAN[N]))$
```

(ROW TO COL CONVERSION MADE)

(E26) $$VE_A = \begin{bmatrix} 3.2068121E-2 \\ 2.3563655\ \%I \\ -9.2678274 \end{bmatrix}$$

(ROW TO COL CONVERSION MADE)

(E27) $$VE_B = \begin{bmatrix} -(-1.6291615E-2 + 1.0203168\ \%I) \\ -(1.2919328E-2 + 1.2866464\ \%I) \\ -(-6.3610957 + 3.7252903E-9\ \%I) \end{bmatrix}$$

(E28) $$NE_A = -4.1973244E-2$$

(E29) $$NE_B = -2.0153166E-2 + 1.2644961E-11\ \%I$$

(E30) $$SIGMAN_N = \begin{bmatrix} -2.5642208E-2 & 2.4695094E-2 + 1.0000477\ \%I & 4.9390187E-3 - 5.215057\ \%I \\ 2.4695094E-2 - 1.0000477\ \%I & -2.5642208E-2 & 4.9390187E-3 + 5.215057\ \%I \\ 4.9390187E-3 + 5.215057\ \%I & 4.9390187E-3 - 5.215057\ \%I & -45.414237 \end{bmatrix}$$

```
(C31) DOAIL:FALSE$
(C32) CCELECEVN:EV(CCELTOT,EVAL,FLOAT)$
(C33) KILL(CCELTOT)$
Substitution of numerical values into the expression for the coupling coefficient:
(C34) DISPTERMS(CCELECEVN);
+

1.6342976E-8 CONVEC

        (([-1.2610264, 1, 7.6955511E-2] . [ 3.2068121E-2 ; 2.3563655 %I ; -9.2678274 ])
                ([1, 1, 0.2] . ([ -2.5642208E-2 , 2.4695094E-2 + 1.0000477 %I , 4.9390187E-3 - 5.215057 %I ;
                                  2.4695094E-2 - 1.0000477 %I , -2.5642208E-2 , 4.9390187E-3 + 5.215057 %I ;
                                  4.9390187E-3 + 5.215057 %I , 4.9390187E-3 - 5.215057 %I , -45.414237 ]
                . [ -(-1.6291615E-2 + 1.0203168 %I) ; -(1.2919328E-2 + 1.2866464 %I) ; -(-6.3610957 + 3.7252903E-9 %I) ])) TERM1
        + ([1, 1, 0.2] . ([ -2.5642208E-2 , 2.4695094E-2 + 1.0000477 %I , 4.9390187E-3 - 5.215057 %I ;
                            2.4695094E-2 - 1.0000477 %I , -2.5642208E-2 , 4.9390187E-3 + 5.215057 %I ;
                            4.9390187E-3 + 5.215057 %I , 4.9390187E-3 - 5.215057 %I , -45.414237 ]
        . [ 3.2068121E-2 ; 2.3563655 %I ; -9.2678274 ])) ([2.2610264, 0, 0.12104649] . [ -(-1.6291615E-2 + 1.0203168 %I) ; -(1.2919328E-2 + 1.2866464 %I) ; -(-6.3610957 + 3.7252903E-9 %I) ]) TERM2)

3.0022047E-5 CONTIN (-4.1973244E-2 ([1, 1, 0.2] . [ -(-1.6291615E-2 + 1.0203168 %I) ; -(1.2919328E-2 + 1.2866464 %I) ; -(-6.3610957 + 3.7252903E-9 %I) ])
        ([1, 1, 0.2] . ([ -2.5642208E-2 , 2.4695094E-2 + 1.0000477 %I , 4.9390187E-3 - 5.215057 %I ;
                          2.4695094E-2 - 1.0000477 %I , -2.5642208E-2 , 4.9390187E-3 + 5.215057 %I ;
                          4.9390187E-3 + 5.215057 %I , 4.9390187E-3 - 5.215057 %I , -45.414237 ]
        . 0.57479004 [1, 1, 0.2])) TERM1 + (-2.0153166E-2 + 1.2644961E-11 %I) ([1, 1, 0.2] . [ 3.2068121E-2 ; 2.3563655 %I ; -9.2678274 ])
        ([1, 1, 0.2] . ([ -2.5642208E-2 , 2.4695094E-2 + 1.0000477 %I , 4.9390187E-3 - 5.215057 %I ;
                          2.4695094E-2 - 1.0000477 %I , -2.5642208E-2 , 4.9390187E-3 + 5.215057 %I ;
                          4.9390187E-3 + 5.215057 %I , 4.9390187E-3 - 5.215057 %I , -45.414237 ]
        . 0.57479004 [1, 1, 0.2])) TERM2)

3.0022047E-5 FLOWCUR (-4.1973244E-2 ([1, 1, 0.2] . [ -(-1.6291615E-2 + 1.0203168 %I) ; -(1.2919328E-2 + 1.2866464 %I) ; -(-6.3610957 + 3.7252903E-9 %I) ]) TERM1
                + (-2.0153166E-2 + 1.2644961E-11 %I) ([1, 1, 0.2] . [ 3.2068121E-2 ; 2.3563655 %I ; -9.2678274 ]) TERM2)

1.2601227E-6 (-2.0153166E-2 + 1.2644961E-11 %I)

        ([1, 1, 0.2] . ([ -2.5642208E-2 , 2.4695094E-2 + 1.0000477 %I , 4.9390187E-3 - 5.215057 %I ;
                          2.4695094E-2 - 1.0000477 %I , -2.5642208E-2 , 4.9390187E-3 + 5.215057 %I ;
                          4.9390187E-3 + 5.215057 %I , 4.9390187E-3 - 5.215057 %I , -45.414237 ]
        . [1, 1, 0.2])) PRESSURE

(D34)                                   DONE
```

Fig. VI-12. (continued)

```
(C35) ANSE:EV(CCELECEVN,DOALL,EXPAND,FLOAT);

(ROW TO COL CONVERSION MADE)
(ROW TO COL CONVERSION MADE)
(ROW TO COL CONVERSION MADE)
(D35) 4.6080382E-8 PRESSURE - 2.8912808E-17 %I PRESSURE + 1.6764616E-6 CONTIN TERM1 - 3.0319546E-6 %I CONTIN TERM1
                   + 7.2842154E-7 CONVEC TERM1 - 2.223024E-6 %I CONVEC TERM1 - 1.6074017E-6 FLOWCUR TERM1
                   + 2.9070568E-6 %I FLOWCUR TERM1 - 1.1494268E-6 CONTIN TERM2 + 1.4869468E-6 %I CONTIN TERM2
                   + 1.1101501E-6 CONVEC TERM2 - 3.1740891E-6 %I CONVEC TERM2 + 1.1020775E-6 FLOWCUR TERM2
                   - 1.4256937E-6 %I FLOWCUR TERM2

(C38) ANSET:SUBST([TERM1=1,TERM2=1,CONVEC=1,FLOWCUR=1,PRESSURE=1,CONTIN=1],ANSE);
(D38)                                  1.9063626E-6 - 5.4607579E-6 %I
```

The calculation is repeated for the ion species, energies calculated, and then the results for the growth rates are found:

```
(C101) GAMMA;
                                        2.0520211E-4 E  Q
                                                      A
(D101)                                  ---------------
                                            ME  C
                                              S

(C102) RELGROWTH;
                                        0.21667072 E
                                                   A
(D102)                                  ------------
                                         BO  C
                                           S
```

Fig. VI-12. (concluded)

b. Coupling Coefficients for a Magnetized Plasma

The analytic calculation of nonlinear coupling coefficients for a magnetized plasma introduces several new difficulties that are not encountered in the unmagnetized case. The approximate dispersion relations describing different oscillations in a magnetized plasma, such as lower hybrid waves or magnetosonic waves, are generally more complex. This makes it less practical to eliminate variables by using the dispersion relation. Also, the conductivity tensor is no longer diagonal and its elements may be relatively large if a model including temperature is used. The ideal approach to deriving a simple model would be to use an electrostatic approximation, where valid, and expand the conductivity tensor for the plasma either in $\frac{\omega}{\omega_c}$ or $\frac{\omega_c}{\omega}$ $\left(\omega_c = \frac{qB_o}{m}\right)$, depending on which is appropriate for the species being considered. Then approximate dispersion relations could be used to eliminate variables, and the result ordered in terms of mass ratios of the species. If this calculation were done in a controlled and careful way, much insight could be gained into the physical mechanisms involved.

We have not yet fully explored this procedure to determine possible difficulties. To get immediate results, the calculation has been carried out seminumerically for several cases (see Sec. VI-A.3). The specific cases considered were the coupling of lower hybrid waves to ion acoustic, electrostatic-ion-cyclotron, or magnetosonic waves. The first task was to normalize the general expression for the coupling coefficient and the approximate dispersion relations for the regime of interest. Hence

$$\underline{\omega} = \frac{\omega}{\omega_{ci}}, \quad \underline{k} = \frac{\bar{k}c_S}{\omega_{ci}}.$$

Next a small program was set up to calculate unspecified parameters numerically. For

example, there are three frequency-wavevector pairs: $(\omega_{LH1}, \bar{k}_{LH1})$, $(\omega_{LH2}, \bar{k}_{LH2})$, $(\omega_{LF}, \bar{k}_{LF})$ — or 12 variables. Seven of these can be eliminated by using

$$D(\omega_{LH1}, \bar{k}_{LH1}) = 0$$

$$D(\omega_{LH2}, \bar{k}_{LH2}) = 0$$

$$D(\omega_{LF}, \bar{k}_{LF}) = 0$$

$$\bar{k}_{LH1} = \bar{k}_{LH2} + \bar{k}_{LF}$$

$$\omega_{LH1} = \omega_{LH2} + \omega_{LF},$$

where LH1 and LH2 designate lower hybrid waves, and LF a low-frequency wave. Hence 5 parameters must be specified in order to determine all pairs completely.

Once this is done, the normalized coupling coefficient can be evaluated numerically. During this calculation, it is desirable to keep track of various nonlinear terms (convective, Lorentz, and so forth) and of quantities such as velocities and densities of various waves. This is accomplished by the boxing technique, whereby boxes surrounding particular terms are successively removed at each step in the calculation. With the full details of the calculation available, any of the physically important quantities can be read off from the results. A typical use of this technique is shown in Fig. VI-12. Energies for two of the waves are calculated, and then all of the quantities necessary for evaluating growth rate of a particular case are available. Use of these results in arriving at a physical model for the interaction is discussed in Sec. VI-A.3.

References

1. A. Bers, J. L. Kulp, and D. C. Watson, "Analytic Studies of Nonlinear Plasma Problems by Symbolic Manipulation Programs on a Computer," Quarterly Progress Report No. 108, Research Laboratory of Electronics, M.I.T., January 15, 1973, pp. 167-185.

3. PARAMETRIC EXCITATION OF ION WAVES BY WAVES NEAR THE LOWER HYBRID FREQUENCY

National Science Foundation (Grant GK-28282X1)

C. F. F. Karney, A. Bers, J. L. Kulp

Introduction

Considerable interest has been shown recently in schemes for heating a plasma by parametric interactions. This involves exciting a high-frequency plasma wave (the pump) strongly enough that it transfers its energy into lower frequency waves which, it is hoped, can then heat the ions of the plasma. We look at the case with the pump a wave at or above the lower hybrid frequency. That this wave can be efficiently and conveniently excited has already been shown.[1, 2] Parametric excitation of modes near the ion cyclotron frequency with such a pump has also been observed.[3] In the work reported here, we treat this problem by the coupling of modes[4] for an infinite homogeneous plasma.

Much of this work was carried out on MACSYMA[5] and as such it is part of a general effort to evaluate the role of symbolic manipulation by computers in the field of plasma physics. Details of techniques developed on MACSYMA for this particular problem are described in Sec. VI-A. 2.

Linear Modes

We consider coupling from waves near the lower hybrid frequency to the following modes: ion acoustic, electrostatic ion cyclotron, and magnetosonic. First, we look briefly at the derivation of approximate dispersion relations for these modes.

The plasma that we consider is homogeneous with a uniform magnetic field in the z direction. The ions are assumed cold. The β of the plasma is taken to be very small; for the purposes of the numerical calculations we take $\omega_{pi}/\Omega_i = 10(\approx c/c_A)$, where c is the velocity of light, and c_A is the Alfvén velocity, $c_A/c_S = 10^3$, where c_S is the ion sound velocity, and $m_e/m_i = 1837$. We use the fluid equations in the electrostatic limit, and choose $(\omega, \bar{k})$ so that Landau and cyclotron damping are small.

a. Ion Acoustic and Lower Hybrid Modes

For electrostatic modes we may write the dispersion relation as

$$K_\ell \triangleq \frac{\bar{k} \cdot \bar{\bar{K}} \cdot \bar{k}}{k^2} = 0, \tag{1}$$

where $\bar{\bar{K}} = \bar{\bar{I}} + \frac{i\bar{\bar{\sigma}}}{\omega\epsilon_o}$. Furthermore, we note that for ion acoustic modes and lower hybrid

type resonances $\Omega_e \gg \omega \gg \Omega_i$, so we say that the electrons see an infinite magnetic field and the ions, zero magnetic field, in which case

$$K_\ell \cong 1 - \frac{k_\parallel^2}{k^2} \frac{\omega_{pe}^2}{\omega^2 - v_{Te}^2 k_\parallel^2} - \frac{\omega_{pi}^2}{\omega^2} = 0 \tag{2}$$

or

$$1 - \frac{\overset{v}{k}{}_\parallel^2}{\overset{v}{k}{}^2} \frac{\mu \overset{v}{\omega}{}_{pi}^2}{\overset{v}{\omega}{}^2 - \mu \overset{v}{k}{}_\parallel^2} - \frac{\overset{v}{\omega}{}_{pi}^2}{\overset{v}{\omega}{}^2} = 0. \tag{3}$$

Here we have introduced the following normalizations: $\overset{v}{k} \triangleq kc_S/\Omega_i$, $\overset{v}{\omega} \triangleq \omega/\Omega_i$, $\mu \triangleq m_i/m_e$. Then we may obtain the ion acoustic wave by taking $\overset{v}{k}{}_\parallel^2 \gg \overset{v}{\omega}{}^2/\mu$ and $\overset{v}{k}{}^2 \ll \overset{v}{\omega}{}_{pi}^2$ to obtain

$$\overset{v}{\omega}{}^2 = \overset{v}{k}{}^2. \tag{4}$$

We obtain the lower hybrid wave by putting $\overset{v}{k}{}_\parallel^2 \ll \overset{v}{\omega}{}^2/\mu$ and $\frac{\overset{v}{k}{}_\parallel^2}{\overset{v}{k}{}^2} \ll \frac{1}{\mu}$ to obtain

$$\overset{v}{\omega}{}^2 = \overset{v}{\omega}{}_{pi}^2. \tag{5}$$

The lower hybrid wave may be extended to higher frequencies if we make $\frac{\overset{v}{k}{}_\parallel^2}{\overset{v}{k}{}^2} \gg \frac{1}{\mu}$, in which case

$$\overset{v}{\omega}{}^2 = \overset{v}{\omega}{}_{pi}^2 \, \mu \frac{k_\parallel^2}{k^2}. \tag{6}$$

Allowing $\frac{\overset{v}{k}{}_\parallel^2}{\overset{v}{k}{}^2}$ to be arbitrary gives

$$\overset{v}{\omega}{}^2 = \overset{v}{\omega}{}_{pi}^2 \left(1 + \frac{\mu \overset{v}{k}{}_\parallel^2}{\overset{v}{k}{}^2}\right). \tag{7}$$

We may conveniently plot these conditions on the validity of the dispersion relation on a $\overset{v}{k}_\perp$, $\overset{v}{k}_\parallel$ diagram (see Figs. VI-13 and VI-14). For simplicity, the regions have been extended to the point where the inequalities are equalities.

Electron Landau damping is a maximum when

$$\frac{k_{\parallel}^2}{\omega^2} v_{Te}^2 \sim 1$$

or

$$\frac{\overset{\vee}{k}_{\parallel}^2}{\overset{\vee}{\omega}^2} \mu \sim 1,$$

so we avoid this by taking $\overset{\vee}{k}_{\parallel}^2 \ll \overset{\vee}{\omega}^2/\mu$ or $\overset{\vee}{k}_{\parallel}^2 \gg \overset{\vee}{\omega}^2/\mu$.

Ion cyclotron damping will occur if the ions are warm; this damping is strong when $\frac{k_{\parallel} v_{Ti}}{\omega - \Omega_i} \sim 1$. We may avoid this region by making θ sufficiently large, consistent with avoiding electron Landau damping.

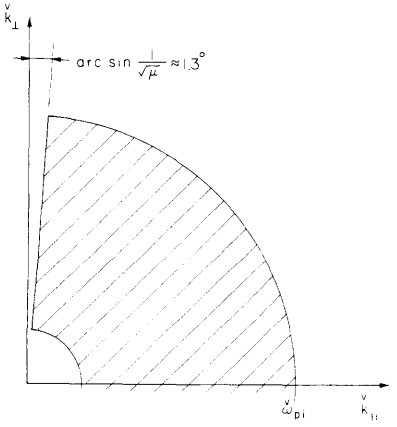

Fig. VI-13. Region of validity of ion acoustic dispersion relation $\overset{\vee}{\omega}^2 = \overset{\vee}{k}^2$.

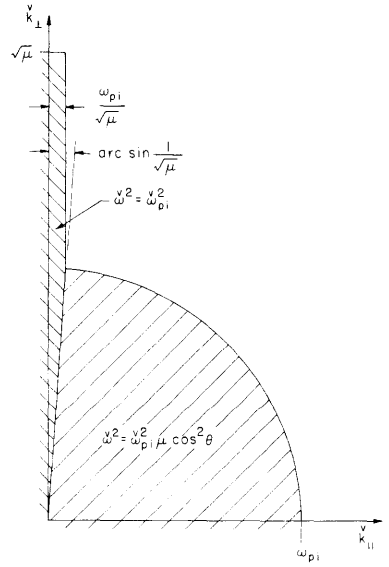

Fig. VI-14. Region of validity of dispersion relations for lower hybrid type waves.

b. Magnetosonic Modes

These are modes with $\Omega_i > \omega$. If we choose $\Omega_i \cos\theta \gg \omega$, we may say that both the ions and the electrons see an infinite magnetic field. The electrostatic dispersion relation now becomes approximately

$$K_\ell \cong 1 - \frac{\overset{v}{k}_{||}^2}{\overset{v}{k}^2} \frac{\overset{v}{\omega}_{pe}^2}{\overset{v}{\omega}^2 - \mu \overset{v}{k}_{||}^2} - \frac{\overset{v}{k}_{||}^2}{\overset{v}{k}^2} \frac{\overset{v}{\omega}_{pi}^2}{\overset{v}{\omega}^2} = 0. \tag{8}$$

Then with $\overset{v}{k}_{||}^2 \gg \overset{v}{\omega}^2/\mu^2$ and $\overset{v}{k}^2 \ll \overset{v}{\omega}_{pi}^2$ we obtain

$$\overset{v}{\omega}^2 = \overset{v}{k}_{||}^2. \tag{9}$$

The region of validity is given by $\overset{v}{k}_{||}^2 \ll 1$ and $\overset{v}{k}_{\perp}^2 \ll 1$ (see Fig. VI-15).

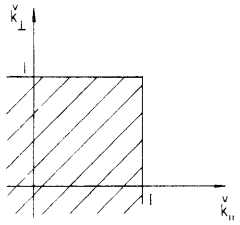

Fig. VI-15. Region of validity of magnetosonic dispersion relation $\overset{v}{\omega} = k_{||}$.

For $T_e \gg T_i$ this mode avoids Landau and ion cyclotron damping. We must avoid regions where $\overset{v}{k}_{||} \ll 1$, for then $\overset{v}{\omega} \ll 1$ and in any real plasma there are drift modes at these low frequencies.

c. Electrostatic Ion Cyclotron Modes

In this case we make the usual infinite magnetic-field approximation for the electrons, but no approximations for the ions. Then

$$K_\ell \cong 1 - \frac{\overset{v}{k}_{||}^2}{\overset{v}{k}^2} \frac{\overset{v}{\omega}_{pe}^2}{\overset{v}{\omega}^2 - \mu \overset{v}{k}_{||}^2} - \frac{\overset{v}{\omega}_{pi}^2}{\overset{v}{k}^2} \left[\frac{\overset{v}{k}_{\perp}^2}{\overset{v}{\omega}^2 - 1} + \frac{\overset{v}{k}_{||}^2}{\overset{v}{\omega}^2} \right] = 0. \tag{10}$$

If $\overset{v}{k}_{||}^2 \gg \frac{\overset{v}{\omega}^2}{\mu}$ and $\overset{v}{k}^2 \ll \overset{v}{\omega}_{pi}^2$, we solve for ω and obtain

$$\overset{v}{\omega}^2 = \frac{1}{2} \left[1 + \overset{v}{k}^2 \pm \sqrt{(1+\overset{v}{k}^2)^2 - 4\overset{v}{k}_{||}^2} \right]. \tag{11}$$

For the electrostatic ion cyclotron mode we choose the upper sign (see Fig. VI-16). The lower sign corresponds to the magnetosonic branch and its resonance. The conditions that Landau and cyclotron damping be small are $\overset{v}{k}_{||}^2 \gg \frac{\overset{v}{\omega}^2}{\mu}$ and $\frac{k_{||}^2 v_{Ti}^2}{(\omega - \Omega_i)^2} \ll 1$,

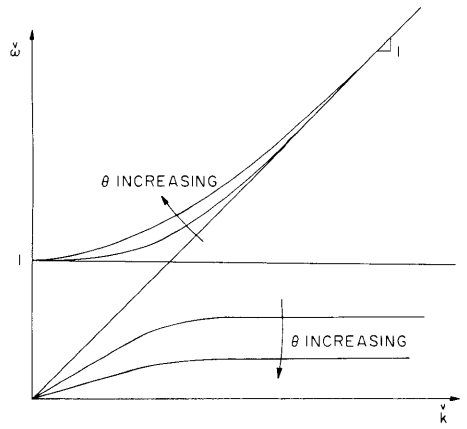

Fig. VI-16. Dispersion diagram for waves near the ion cyclotron frequency.

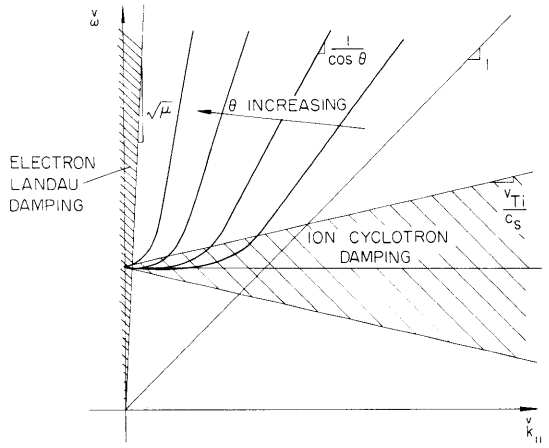

Fig. VI-17. Regions where electrostatic ion cyclotron waves are damped.

respectively. These are plotted on an $\check{\omega}, \check{k}_{\parallel}$ diagram in Fig. VI-17. As long as we avoid the region of electron Landau damping (say, $90° > \theta > 87°$), the larger we can choose θ, the better off we are. Here we can find weakly damped modes even for $T_e \sim T_i$.

Resonance Conditions

We look for 3 modes satisfying the "resonance conditions"

$$\bar{k}_n = \bar{k}_a + \bar{k}_b \tag{12}$$

$$\omega_n = \omega_a + \omega_b. \tag{13}$$

The convention that we adopt is as follows: a is the pump driven externally, b is an "idler" mode, and n is the signal (some low-frequency mode that we are trying to excite). We normally have the magnitude of the pump frequency greater than those of the other two modes $\omega_a > |\omega_b|, |\omega_n|$. Since we choose $\omega_a > 0$, we shall have $\omega_b < 0$.

The first step in satisfying the resonance conditions is obviously to decide what class of modes we wish to couple. In our case we examine the coupling of:

One resonance near the lower hybrid frequency with (i) two ion acoustic waves.

Two resonances near the lower hybrid frequency with (ii) an electrostatic ion cyclotron mode or (iii) a magnetosonic mode.

We shall use the approximate dispersion relations already derived, as this relieves us of the necessity of having to solve high-order polynomials.

Now we have 12 unknowns (the $\bar{k}$ and the ω of the three modes) with 7 equations

(4 resonance conditions and 3 dispersion relations), and so there are 5 free parameters that we may choose. Only 4 of these are nontrivial, however, since the fifth amounts to nothing more than a choice of axes; hence, we always take the pump to lie in the x, z plane. Having chosen these five parameters, we may calculate $\bar{k}, \omega$ for each mode. Finally, we should go back and check to see that our approximations were valid.

a. Coupling to Two Ion Acoustic Waves

We note that for the pump $\overset{v}{\omega}_a > \overset{v}{\omega}_{pi}$, and for ion acoustic waves $\overset{v}{\omega}^2_{b,n} \ll \overset{v}{\omega}^2_{pi}$. Remembering that $\overset{v}{\omega}_n = \overset{v}{\omega}_a + \overset{v}{\omega}_b$, we see that the second inequality is best satisfied if $|\overset{v}{\omega}_{b,n}| \approx \overset{v}{\omega}_a/2$ and $\overset{v}{\omega}_a \approx \overset{v}{\omega}_{pi}$. Thus we use the dispersion relation $\overset{v}{\omega}_a = \overset{v}{\omega}_{pi}$ for the pump (valid for $\cos^2\theta_a \ll \frac{1}{\mu}$). For mode b and n we use $\overset{v}{\omega}_b = -|\overset{v}{\bar{k}}_b|$, $\overset{v}{\omega}_n = |\overset{v}{\bar{k}}_n|$. We begin by choosing $\bar{k}_a$ (remember $k_{ay} = 0$ and $\cos^2\theta_a \ll \frac{1}{\mu}$). Then $\overset{v}{\bar{k}}_n + (-\overset{v}{\bar{k}}_b) = \overset{v}{\bar{k}}_a$, and $\overset{v}{\omega}_n + (-\overset{v}{\omega}_b) = \overset{v}{\omega}_a$, or $|\overset{v}{\bar{k}}_n| + |-\overset{v}{\bar{k}}_b| = \overset{v}{\omega}_a$. Thus the locus of $\overset{v}{\bar{k}}_n$ is an ellipsoid with $\overset{v}{\bar{k}}_a$ spanning the foci (see Fig. VI-18). Note, however, that certain regions are forbidden to $\overset{v}{\bar{k}}_n$ and $\overset{v}{\bar{k}}_b$, since

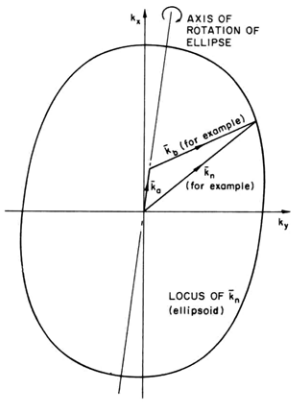

Fig. VI-18. Locus of $\bar{k}_n$ for a given $\bar{k}_a$ for the case of coupling to two ion acoustic waves.

the dispersion relation is no longer valid (see Fig. VI-13). Then $\overset{v}{\bar{k}}_b$ and $\overset{v}{\bar{k}}_n$ are determined by choice of, say, $\hat{k}_n$ (the direction cosines of $\bar{k}_n$).

Thus the five parameters that we choose in this case are axes ($k_{ay} = 0$), k_{ax}, k_{az} and $\hat{k}_n$.

b. Coupling to Electrostatic Ion Cyclotron Mode

In this case we consider the pump above the lower hybrid frequency, an idler nearby (in magnitude of frequency) and the signal, an electrostatic ion cyclotron mode, at a considerably lower frequency.

We describe the pump and the idler (modes a and b) by Eq. 7. Since $\omega_n \ll \omega_a$, $\omega_b \approx -\omega_a$ and $\cos^2\theta_a \approx \cos^2\theta_b$. There are two possibilities: either the z components of

k_a and k_b are of opposite sign, or they have the same sign. The possibilities are shown in Fig. VI-19. Note that in the first case (Fig. VI-19a) k_{az} is much larger than in the

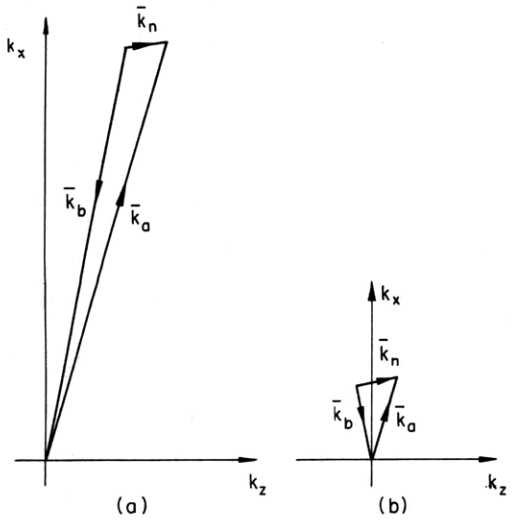

Fig. VI-19.

Two possible configurations for coupling to electrostatic ion cyclotron modes. (ω_a and $\bar{k}_n$ are assumed fixed.)
(a) k_{az} and k_{bz} have opposite signs.
(b) k_{az} and k_{bz} have the same sign.

second case (Fig. VI-19b) for a given $\bar{k}_n$ and pump frequency, and so the pump in the first case is far more likely to be electron Landau damped. Note that we cannot take k_{nz} arbitrarily small, otherwise the wave is ion-cyclotron damped; see Fig. VI-17. For this reason, the method illustrated in Fig. VI-19b is preferred. Similar considerations usually force us to take $\nu\omega_a$ considerably above $\nu\omega_{pi}$ (we cannot take it too high, however, or the efficiency of the down-conversion is impaired); typically we take $\nu\omega_a/\nu\omega_{pi} = 2.5$. Therefore $\cos^2\theta_a \gg \frac{1}{\mu}$ in all cases that we consider; contrast this with the case of coupling to two ion acoustic modes where we must take $\cos^2\theta_a \ll \frac{1}{\mu}$.

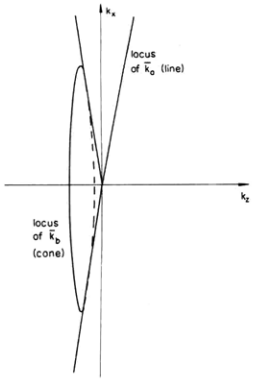

Fig. VI-20. Loci of $\bar{k}_a$ and $\bar{k}_b$ for coupling to an electrostatic ion cyclotron mode.

We may choose the following parameters: $k_{ay} = 0$, ω_a, and $\bar{k}_n$. From ω_a we calculate θ_a (choosing it in the quadrant 0-90°) so $\bar{k}_a$ can lie anywhere on a line (Fig. VI-20).

From $\bar{k}_n$ we can calculate ω_n, using the dispersion relation (Eq. 11), and hence ω_b, using the resonance condition (Eq. 13). From ω_b we can calculate θ_b, and $-\bar{k}_b$ can lie anywhere on a cone (Fig. VI-20). Using the resonance condition $\bar{k}_n = \bar{k}_a + \bar{k}_b$, we can easily find $\bar{k}_a$ and $\bar{k}_b$.

c. Coupling to Magnetosonic Waves

Arguments very similar to those used in the previous case may be applied here. The reason why we may not take $\check{k}_{nz}$ arbitrarily small is different; in this case, if we did, $\check{\omega}_n$ would also be small and the efficiency of the energy conversion would be very poor.

Calculation of Coupling Coefficient

The procedure is as follows for the calculation of the coupling coefficient M, where[4]

$$M = \frac{\bar{E}_n \cdot \bar{J}_n^{(2)}}{\omega_n}. \tag{14}$$

We begin by calculating numerical values of M exactly for a number of cases. From these we identify the dominant terms in the interaction, and then attempt to derive a good analytic approximation for M.

The first task – that of calculating M numerically – was chiefly carried out on MACSYMA.[5] This required symbolically manipulating the general expression for M into a suitable form so that numbers could easily be substituted. The substitution and evaluation were also carried out on MACSYMA. Several techniques developed for these purposes are described in detail in Sec. VI-A. 2. Here we merely quote the conclusions of these evaluations.

Note that, in general, we would also have to calculate the coupling coefficient giving the excitation of the idler by the pump and signal before we could solve for a growth rate. For synchronous loss-free interactions that we are considering, however, the coupling coefficients are equal.

a. Coupling to Ion Acoustic Waves

Significant cancellations occur here: (i) the ion flow-current and convective terms; (ii) the electron continuity and flow-current terms; and (iii) in the electron term the sum of continuity and flow-current terms with the convective term.[5]

Consider a very rough scheme for ordering the terms. To do this, we take the ions to be unmagnetized and the electrons fully magnetized. We also ignore the electron pressure for the pump (the lower hybrid resonance is a cold-plasma mode), as well as the electron inertia for the ion acoustic modes. Finally, we concentrate only the very large or very small factors in any one term; in the former category, we include the

mass ratio μ, and in the latter $\frac{\check{k}_a}{\check{\omega}_a} \triangleq \epsilon_1$ and $\cos\theta_a \triangleq \epsilon_2$.

The velocities and densities for each mode are ordered as follows. (Note that for these purposes we have replaced $\bar{E}$ with $\bar{k}$.)

$$v_{ai} = \frac{\check{k}_a}{\check{\omega}_a} \sim \epsilon_1 \qquad v_{ae} = -\mu \frac{\check{k}_{za}}{\check{\omega}_a}\hat{z} \sim \mu\epsilon_1\epsilon_2$$

$$v_{bi} = \frac{\check{k}_b}{\check{\omega}_b} \sim 1 \qquad v_{be} = -\sin\theta_b\hat{z} \sim 1$$

$$n_{ai} = \frac{\check{k}_a^2}{\check{\omega}_a^2} \sim \epsilon_1^2 \qquad n_{ae} = -\mu \frac{\check{k}_{za}^2}{\check{\omega}_a^2} \sim \mu\epsilon_1^2\epsilon_2^2$$

$$n_{bi} = \frac{\check{k}_b^2}{\check{\omega}_b^2} \qquad n_{be} \sim 1.$$

(Remember $\hat{v}_{ae} = \hat{v}_{be} = \hat{z}$, whereas $\hat{v}_i = \hat{k}$.) Substituting these in our expression for M, we find

electron flow current $\sim \mu\epsilon_1\epsilon_2$

electron continuity $\sim \mu\epsilon_1\epsilon_2$

electron convective $\sim \epsilon_1\epsilon_2$

electron pressure $\sim \mu\epsilon_1^2\epsilon_2^2$

ion flow current $\sim \epsilon_1$

ion convective $\sim \epsilon_1$.

To find the results of the cancellations, improvements will have to be made in the approximations. We find that

electron flow current + continuity $\sim \frac{\text{flow current}}{\mu} \sim \epsilon_1\epsilon_2$

electron flow current + continuity + convective $\sim \epsilon_1^2\epsilon_2^2$

ion flow current + convective $\sim \epsilon_1^2$.

To find the dominant term we compare the electron pressure, the electron flow-current + continuity + convective, and the ion flow-current + convective terms. We see quickly that of these, the ion term is the largest, since in satisfying the resonance conditions we are required to take $\mu \cos^2 \theta_a = \mu\epsilon_2^2 \ll 1$.

The cancellation between flow-current and continuity terms is of great importance in this interaction; and since it also appears in the other interactions that we consider, we examine the reasons for it.

The flow-current term $n_1\bar{v}_1$, besides contributing directly to the coupling coefficient, is also the driving term for the continuity equation (specifically, its divergence is), and this gives rise to the continuity term $\nabla \cdot (n_1\bar{v}_1)$. Now, $\nabla \cdot (n_1\bar{v}_1)$ can be thought of as a creation of electron fluid which, if the rest of the electron fluid were stationary, would lead to density fluctuations. For ion acoustic modes, however, pressure dominates over inertia, so the electron fluid is not stationary; on the contrary, it moves in such a way as nearly to cancel out density fluctuations. So the response of the plasma to a continuity driving term is to produce currents that nearly cancel the flow-current term.

The other cancellations are not so interesting, and result primarily from the geometry of the interaction (namely, $\bar{k}_n \approx \bar{k}_b$ and $|\bar{k}_a| \ll |\bar{k}_n|$).

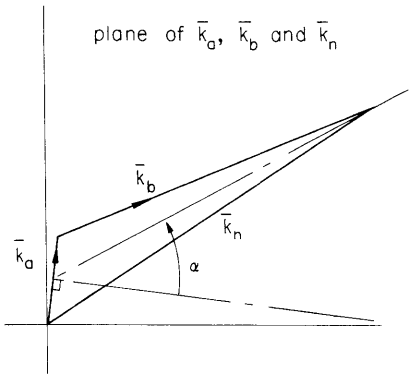

Fig. VI-21. Definition of angle α.

To obtain an analytic expression for the ion contribution to M, we make the approximation $B_o = 0$ for the ions. This is a good approximation when the flow-current or convective terms are considered separately. Because of the cancellation, however, the imaginary part of M_{ion} (the result of finite B_o effects) is not negligible, and for some interactions of this type it may be necessary to include these finite B_o effects.

Carrying out the derivation of M_{ion} as outlined, and keeping only terms of lowest order in $k_a/\omega_a, (\epsilon_1)$, we obtain

$$M \approx M_{ion} \approx c\left[\frac{-1}{2\vec{k}_a\vec{k}_b\vec{k}_n\omega_n\mu}\right]\vec{k}_n\,\frac{\vec{v}\,k_a^2}{\vec{v}\,\omega_a^2}\,[1-2\sin^2\alpha], \tag{15}$$

where α is the angle shown in Fig. VI-21, and

$$c = \frac{E_n^* E_a E_b \epsilon_o \omega_{pi}^2}{\Omega_i^3 m_e c_s}.$$

b. Coupling to Electrostatic Ion Cyclotron Waves

As before, we begin by ordering the terms. We make the same approximations for the pump and idler as were made for the pump in the previous case; i.e., that the ions are unmagnetized, and that the electrons are infinitely magnetized and cold. Then we find

$$\text{electron convec} \sim \mu\epsilon_1^2\epsilon_2^2$$

$$\text{electron flowcur} \sim \mu^2\epsilon_1^3\epsilon_2^3$$

$$\text{electron contin} \sim \mu^2\epsilon_1^3\epsilon_2^3$$

$$\text{electron pressure} \sim \mu^2\epsilon_1^4\epsilon_2^4$$

$$\text{ion convec} \sim \epsilon_1^2$$

$$\text{ion flowcur} \sim \epsilon_1^3$$

where, as before, $\epsilon_1 \triangleq \check{k}_a/\check{\omega}_a$, and $\epsilon_2 \triangleq \cos\theta_a$. Again we have

$$\text{electron flowcur + contin} \sim \frac{\text{flowcur}}{\mu} \sim \mu\epsilon_1^3\epsilon_2^3.$$

The electron convective term dominates, since we find $\mu\epsilon_1^2\epsilon_2^2 \ll 1$. Recall that we were forced by the resonance conditions to pick $\mu \cos^2\theta_a = \mu\epsilon_2^2 \gg 1$, and thus we may neglect the ion convective term.

In calculating M we need only include the electron convective term. The additional approximation that we make is $B_o = \infty$. In certain regions, however, this approximation is not adequate and we must include some finite magnetic field effects; it is sufficient to include the $\bar{E} \times \bar{B}$ velocity of modes a and b. Note that although this component of the electron velocity is much less than the z component, it can be accentuated; for instance, when we take $\bar{v}_a \cdot \nabla_b$ (that is, $\bar{v}_a \cdot \bar{k}_b$), if k_b has a large y component and a small z component.

Proceeding as outlined, and keeping only the lowest order terms in ϵ_1 and ϵ_2, we obtain

$$M \approx M_{el,\,convec} \approx c\left[\frac{1}{2\overset{v}{k}_a\overset{v}{k}_b\overset{v}{k}_n\overset{v}{\omega}_n\mu}\right]\left[-\mu\,\frac{\overset{v}{k}_{az}\overset{v}{k}_{bz}}{\overset{v}{\omega}_a\overset{v}{\omega}_b}\,\overset{v}{\omega}_n - i\,\frac{(\overset{v}{\bar{k}}_b\times\overset{v}{\bar{k}}_b)\cdot\hat{z}}{\overset{v}{\omega}_a}\,\overset{v}{\omega}_n\right]. \tag{16}$$

In this expression we identify the real part as the result if we take $B_o = \infty$, and the imaginary part as the finite magnetic field corrections.

c. Coupling to a Magnetosonic Mode

This interaction is very similar to coupling to electrostatic ion cyclotron waves because we have the same two waves (two resonances above the lower hybrid frequency) interacting. The scheme for ordering terms is the same as in the previous case. Taking only the electron convective term, as before, we obtain precisely the same expression for M (Eq. 16).

It should be pointed out that in both cases of coupling from two lower hybrid waves, the dominance of the electron convective term depends on our choice of $\mu\cos^2\theta_a \gg 1$. It may be that in a plasma with slightly different parameters, we may choose $\mu\cos^2\theta_a \sim 1$. In such a case we would have to include the ion convective term in our expression for M.

Calculation of Growth Rate

The growth rate γ for the signal and idler waves is given by

$$\gamma^2 = \frac{-\omega_b\omega_n}{W_bW_n}\,\frac{|M|^2}{16}, \tag{17}$$

where the W are energy densities.

a. Coupling to Two Ion Acoustic Waves

For modes b and n we take $W = \frac{2}{\omega^2}\,\overset{v}{\omega}{}^2_{pi}W_e$, where $W_e = \frac{1}{4}\,\epsilon_o|E|^2$. We have neglected the electron energy here and assumed that the ions are unmagnetized. Then, using our expression for M, we find

$$\frac{\gamma}{\omega_n} = \frac{v_{ai}}{v_{aph}}\,\frac{[1-2\sin^2\alpha]}{4}, \tag{18}$$

where $v_{ai} \triangleq \frac{|E_a|q}{m_i\omega_a}$, $v_{aph} \triangleq \omega_a/k_a$, and α is as defined in Fig. VI-21.

b. Coupling to an Electrostatic Ion Cyclotron Wave

Assuming that the electrons are cold and fully magnetized, we obtain for W_b

$$W_b = 2\mu \frac{\overset{\vee}{\omega}_{pi}^2}{\overset{\vee}{\omega}_b^2} \cos^2 \theta_b W_{eb},$$

where we have ignored the ion energy, and for the signal, with $\sin \theta_n \lesssim 1$,

$$W_n = 2 \frac{\overset{\vee}{\omega}_n^2}{\left(\overset{\vee}{\omega}_n^2 - 1\right)^2} \sin^2 \theta_n \overset{\vee}{\omega}_{pi}^2 W_{en}.$$

Here we have neglected the electron energy.

We may simplify by separating those cases in which the z component of v dominates when taking $v \cdot \nabla$ (i.e., the real part of M) from those wherein the $\bar{E} \times \bar{B}$ component dominates. In the first case

$$\frac{\gamma}{\omega_n} = \left(\frac{-\omega_b}{\omega_n}\right)^{1/2} \frac{v_{a\parallel}}{v_{Te}} \frac{1}{4} \frac{\overset{\vee}{\omega}_n^2 - 1}{\overset{\vee}{k}_{\perp n} \overset{\vee}{\omega}_n}, \tag{19}$$

where $v_{a\parallel} \triangleq \frac{q|E_a| \cos \theta_a}{m_e \omega_a}$. In the second case,

$$\frac{\gamma}{\omega_n} = \left(\frac{-\omega_b}{\omega_n}\right)^{1/2} \frac{v_{a\perp}}{v_{Te} \cos \theta_a} \frac{1}{4} \frac{[\sin \theta_{a,b}]\left(\overset{\vee}{\omega}_n^2 - 1\right)}{\overset{\vee}{k}_{\perp n} \overset{\vee}{\omega}_n}, \tag{20}$$

where $v_{a\perp} \triangleq |E_a|/B_o$, and $\sin \theta_{a,b} \triangleq \frac{(\bar{k}_a \times \bar{k}_b) \cdot \hat{z}}{k_a k_b}$. These expressions may be combined if necessary. We do this by taking the square root of the sum of the squares of the two expressions for γ/ω_n.

c. Coupling to Magnetosonic Waves

In this case the expression for W_n changes. If we consider the ions in mode n to be fully magnetized, and if we ignore the electron energy,

$$W_n = 2 \frac{\cos^2 \theta_n}{\overset{\vee}{\omega}_n^2} \overset{\vee}{\omega}_{pi}^2 W_{en}.$$

With this interaction it is only possible to have the real part of M dominating because $|\bar{k}_n|$ is too small to separate $\bar{k}_a$ and $\bar{k}_b$, when projected on the x, y plane (cf. definition of $\sin \theta_{a,b}$). In this case

$$\frac{\gamma}{\omega_n} = \left(\frac{-\omega_b}{\omega_n}\right)^{1/2} \frac{v_{a\parallel}}{v_{Te}} \frac{1}{4}. \tag{21}$$

d. Thresholds for Instability

The expressions for growth rate that we have obtained are modified when modes b or n are damped, or if there is a frequency mismatch. It is now observed that a certain threshold pump field must be achieved before growth can be obtained. If γ_b and γ_n are the damping rates for modes b and n, respectively, and if the frequency mismatch $(\omega_n - \omega_a - \omega_b)$ is δ_ω, then growth is obtained[4] if

$$\gamma^2 > \gamma_b\gamma_n + \frac{\gamma_b\gamma_n}{(\gamma_b+\gamma_n)^2}\,\delta_\omega^2, \tag{22}$$

where γ is the growth rate previously calculated (i.e., by neglecting damping and frequency mismatch).

References

1. W. M. Hooke and S. Bernabei, Phys. Rev. Letters 28, 407 (1972).
2. R. J. Briggs and R. R. Parker, Phys. Rev. Letters 29, 852 (1972).
3. W. M. Hooke and S. Bernabei, Phys. Rev. Letters 29, 1218 (1972).
4. A. Bers, Notes on Lectures: Linear Waves and Instabilities, given at Ecole d'Eté de Physique Théorique, Les Houches, France, July 1972 (Gordon and Breach, New York, in press).
5. A. Bers, J. L. Kulp, and D. C. Watson, Quarterly Progress Report No. 108, Research Laboratory of Electronics, M. I. T., January 15, 1973, pp. 167-185.

VI. APPLIED PLASMA RESEARCH

D. Laser-Plasma Interactions

Academic and Research Staff

Prof. E. V. George
Prof. A. Bers
Prof. H. A. Haus
Dr. A. H. M. Ross
J. J. McCarthy
W. J. Mulligan

Graduate Students

Y. Manichaikul
J. L. Miller
D. Prosnitz
C. W. Werner
D. Wildman

1. GENERATION AND AMPLIFICATION OF HIGH-INTENSITY, NANOSECOND TEA CO_2 LASER PULSES

National Science Foundation (Grant GK-33843)
U. S. Army – Research Office – Durham (Contract DAHC04-72-C-0044)

Y. Manichaikul

We have reported previously on generation of short nanosecond pulses from a pin resistor TEA CO_2 laser by way of mode locking and cavity dumping.[1] Single pulses 4 ns wide (full width at half maximum, FWHM) with peak power ~1 kW were produced. Problems were encountered with the system and a new one was built. The problems, and the changes that have been made in the new system, are as follows.

(i) The peak power obtained from the previous system was too low for some experiments. For example, to saturate a TEA CO_2 laser amplifier requires a peak power of intensity greater than 100 kW/cm^2. In our new system we use a 3-electrode TEA CO_2 discharge tube which has a higher gain than the pin-resistor TEA CO_2 discharge tube.[2] With this improved system we have obtained mode-locked pulses of peak powers in excess of 500 kW.

(ii) A germanium acousto-optic modulator at Brewster angle is now being used. This eliminates the power-density limitation that arose in the old system, which used an antireflection-coated germanium modulator.

(iii) An antireflection-coated GaAs crystal is now placed outside, rather than inside, the optical cavity, which makes alignment of the cavity less critical. Also, since the antireflection coating of the GaAs crystal was slightly damaged, there is less distortion of the TEM mode when the crystal is outside the cavity.

(iv) In the old system the high-voltage supply to the cavity-dumping GaAs crystal was falsely triggered by electrical noise generated by the laser discharge tube. In the new system a laser-induced spark gap[3] is used to eliminate this problem.

(v) Previously, continuous RF power was supplied to the germanium mode-locking

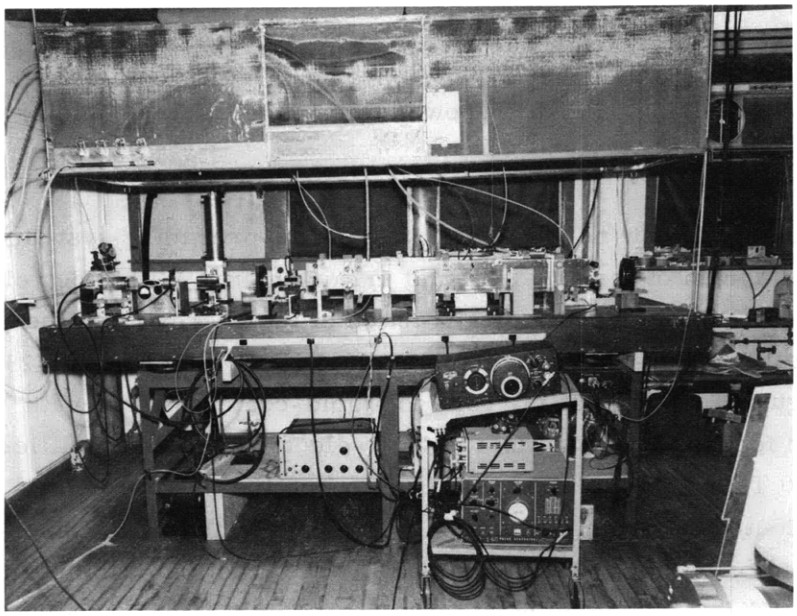

Fig. VI-22.
Photograph of experimental apparatus.

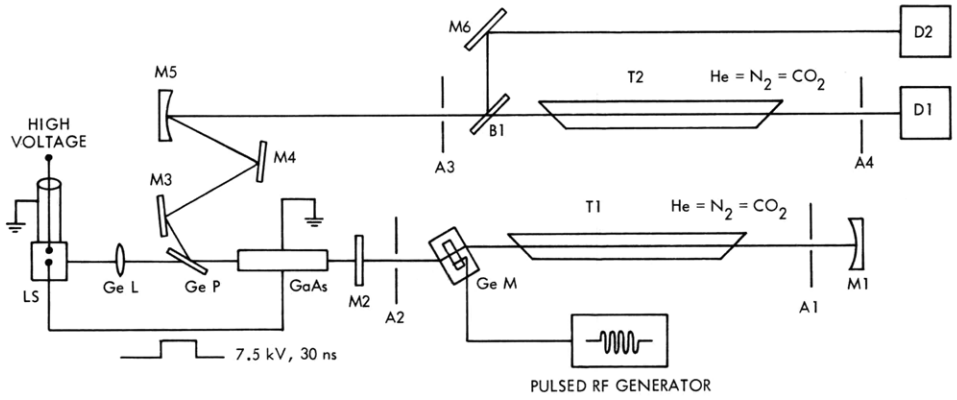

A1, A2, A3, A4	Apertures
B1	NaCl beam splitter
D1	Gold-doped detector
D2	Copper-doped detector
GaAs	Electro-optic modulator
Ge L	Germanium lens, 1.5" focal length
Ge M	Germanium acousto-optic modulator
Ge P	Germanium plate at Brewster angle
LS	Laser-induced spark gap
M1	Gold-coated mirror, 99.6 % reflecting, 4 m radius of curvature
M2	Germanium mirror, 20 % transmitting
M3, M4, M6	Gold-coated flat mirrors, totally reflecting
M5	Gold-coated mirror, 99.6 % reflecting, 2 m radius of curvature
T1, T2	3-electrode discharge tubes, 1 m long

Fig. VI-23. Diagram of experimental arrangement.

crystal. This caused the germanium crystal to heat up, thereby changing its acoustic resonance frequencies. We are now using pulsed RF power to minimize this problem.

Experimental Arrangement

Figure VI-22 is a photograph of the new ns TEA CO_2 laser pulse-producing system, and Fig. VI-23 is a schematic diagram of the experimental arrangement. With a dc voltage of 5 kV across the GaAs electro-optic modulator a fraction of the energy from the beam can be switched out at the Brewster-angle germanium plate (GeP, see Fig. VI-23). This fraction of the beam was guided by two flat mirrors to a gold-coated mirror with 2-m radius of curvature, which focuses the beam inside the 3-electrode laser amplifier. The tube is operated between 10 Torr and 400 Torr. A fraction of the beam, before going into the amplifier, is reflected out from a beam splitter and detected by a copper-doped liquid-helium-cooled detector with a rise time of <1 ns. The fraction of the beam that has passed through the amplifier is detected by a gold-doped liquid-nitrogen-cooled detector with a rise time of ~1 ns.

Experiments

a. Generation of Nanosecond TEA CO_2 Laser Pulses

The laser cavity has an optical length of approximately 1.88 m. To achieve forced mode locking, RF driving power at 2.5 ms with 4 W peak power was supplied to the germanium acousto-optic modulator. The 3-electrode discharge tube inside the cavity is set to trigger at 2 ms after the RF power is on. We have obtained mode-locked pulses < 2 ns wide (FWHM) with a peak power of ~500 kW. Figure VI-24 shows a typical train of mode-locked pulses detected by a copper-doped detector and displayed on a Tektronix 7904 oscilloscope.

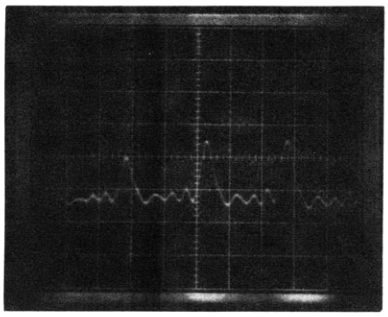

Fig. VI-24.
Typical mode-locked pulses from the laser oscillator (5 ns/div).

The switching out of individual pulses is accomplished by using the laser-induced spark gap, which is normally filled with prepurified nitrogen at 100 psi. The coaxial cable was charged up to 15 kV. We can vary the temporal triggering of this gap by

altering the nitrogen pressure, the distance between the two electrodes of the spark gap, or both. When the spark gap is triggered, a square voltage pulse of 7.5 kV, twice the length of cable, is produced. This pulse is supplied to the GaAs crystal, which rotates the polarization of the desired number of mode-locked pulses. These mode-locked pulses are then reflected out of the train at the Brewster-angle germanium plate.

b. Amplification of Nanosecond TEA CO_2 Laser Pulses

Three pulses from a train of mode-locked pulses were switched out and guided through an amplifier tube. These pulses were measured before and after they propagated through the laser amplifier. Figure VI-25 shows input and output signals detected by

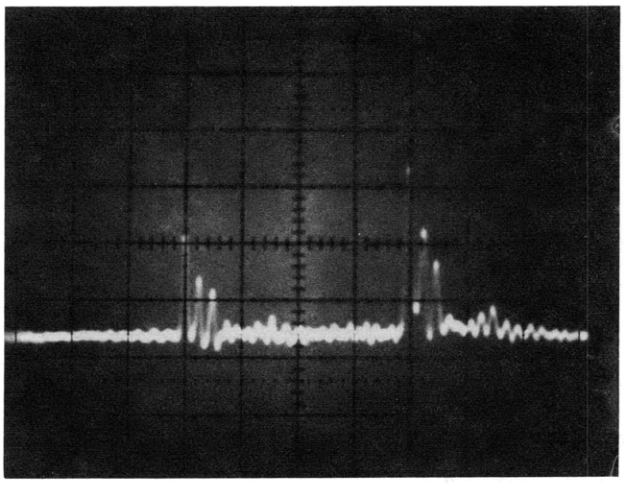

Fig. VI-25.

Input and output pulse trains of the laser amplifier. An artificial 200-ns electrical delay facilitated the display (50 ns/div).

copper-doped and gold-doped germanium detectors, respectively. The output signal from the gold-doped germanium detector was artificially delayed 200 ns by use of a coaxial delay line. By using the add-mode on a Tektronix 454A oscilloscope, we were able to display both signals on a single trace.

In our preliminary studies we have found that the first pulse of our three laser pulses is of sufficient power density to saturate the laser amplifier. Further work on this aspect of the experiment will be described in a future report.

References

1. Y. Manichaikul and E. E. Stark, Jr., Quarterly Progress Report No. 107, Research Laboratory of Electronics, M.I.T., October 15, 1972, pp. 81-84.
2. P. R. Pearson and H. M. Lamberton, "Atmospheric Pressure CO_2 Lasers Giving High Output Energy Per Unit Volume," IEEE J. Quant. Electronics, Vol. QE-8, No. 2, pp. 145-149, February 1972.
3. A. V. Nurmikko, IEEE J. Quant. Electronics, Vol. QE-7, No. 9, pp. 470-471, September 1971.

2. LASER-INDUCED HIGH-FREQUENCY STARK EFFECT IN A PLASMA

National Science Foundation (Grant GK-33843)

D. Prosnitz

There is considerable interest in examining the interactions of an intense laser beam with a plasma. In particular, we wish to study the optical mixing of two lasers in an underdense helium plasma, $\omega_p \ll \omega_\ell$, where $\omega_p^2 = ne^2/m\epsilon_o$, with n, e, m the electron density, charge, and mass, ϵ_o the permittivity of free space, and ω_ℓ the angular frequency of the laser. As reported previously,[1] the high-frequency Stark effect should provide a method of detecting laser-induced plasma instabilities.

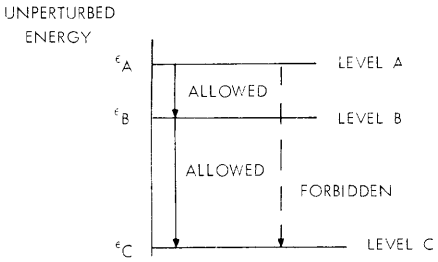

Fig. VI-26. Three-level atom model.

A typical three-level atom is illustrated in Fig. VI-26. Transitions from level A to level B and from B to C are allowed by dipole selection rules, while a transition from A to C is forbidden. The allowed line has a frequency ω_{BC} and the forbidden line a frequency ω_{AC}. Time-dependent perturbation theory predicts that an intense ac electric field will cause two predominant changes in the emission spectra of this three-level system.

(i) The laser field will cause a shift in the frequency of the allowed line.

(ii) The laser field will cause the appearance of additional satellite lines at a frequency ω_s, where $\omega_s = \omega_{AC} \pm \omega_\ell$. Note that satellites may be induced by any oscillating field, including plasma oscillations at ω_p.[2]

The ratio of the intensities of the satellite lines to the allowed line[1,2] is given by

$$S_\pm = \frac{E^2 e^2 a_o^2 R_{AB}}{6} \frac{1}{(\epsilon_A - \epsilon_B \pm \hbar\omega_\ell)^2}, \tag{1}$$

where E is the electric field, a_o is the Bohr radius, ($a_o = \hbar^2/me^2$) is Planck's constant, R_{AB} is a numerical factor representing the dipole strength of transitions between levels A and B, and ϵ_A and ϵ_B are the energy of levels A and B. Obviously, if levels could be found such that $\epsilon_A - \epsilon_B \approx \hbar\omega_\ell$, the satellite line would be greatly enhanced.

If we choose the 10.6 μ radiation (944 cm^{-1}) of a carbon dioxide laser, we find that the 4^3S and 4^3P levels in helium are separated by approximately ω_ℓ. Figure VI-27 illustrates the energy scheme for this interaction. The laser introduces a virtual level slightly

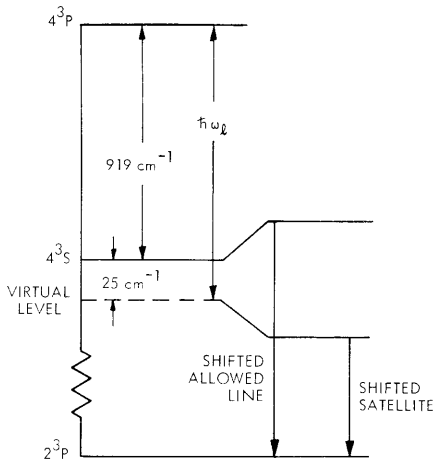

Fig. VI-27.
Partial energy level structure of helium showing predicted satellite transitions.

below the 4^3S level, which causes both the standard Stark repulsion of levels and the satellite emission line. (Note that the level at $4^3P + \omega_\ell$ is not shown, since it is far from resonance and therefore has little effect.)

The experimental apparatus used to observe these effects has been described elsewhere.[1] Figures VI-28 and VI-29 show the observed satellite line. Figure VI-28 demonstrates both the satellite line and the Stark shift of the allowed (4713 Å) line, although the Stark shift is shown with greatly reduced sensitivity. (A small wavelength shift becomes a phase change when observed with synchronous detection techniques.)[1,3] Figure VI-29 demonstrates the pronounced asymmetry of the satellite line. (Instrument resolution was ~0.65 Å in both figures.)

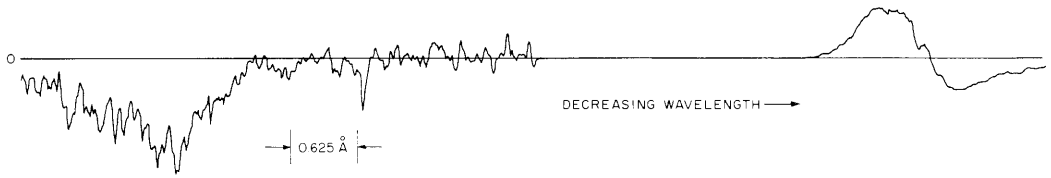

Fig. VI-28. Satellite and high-frequency Stark shift.

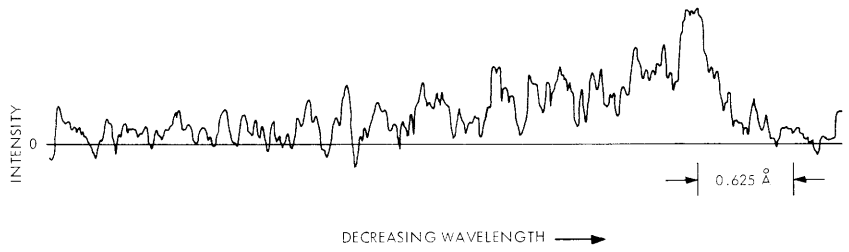

Fig. VI-29. Laser-induced satellite. (Note asymmetry.)

The time development of the satellite is shown in Fig. VI-30, and that of the laser pulse in Fig. VI-31. The satellite time profile was obtained by allowing the 120-ns gate of the boxcar amplifier to scan the signal from the photomultiplier. Equation 1 predicts

that the satellite intensity should be proportional to E^2, or laser power. Figures VI-30 and VI-31 demonstrate that this is qualitatively correct.

Note that Fig. VI-30 is a picture of peak intensity, not of integrated line intensity, as a function of time. This distinction becomes increasingly important at stronger electric field strengths. As laser power increases further, the peak intensity of the satellite

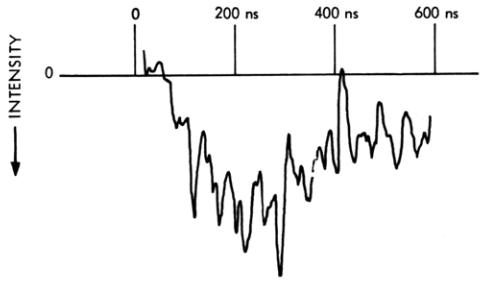

Fig. VI-30. Time development of the satellite.

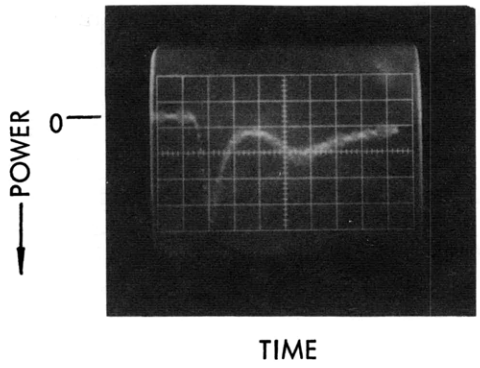

Fig. VI-31. Laser power vs time (200 ns/div).

does not increase, but the spectral line does become much broader (increased integrated intensity) and more asymmetric. Similarly, at lower field strengths the line becomes more symmetric. Figure VI-32 shows the satellite profile produced by an incident laser pulse approximately one-fourth that shown in Fig. VI-29. The increased symmetry (Fig. VI-32) is readily apparent. Note that the integrated intensity of Fig. VI-29 is only twice that of Fig. VI-32, whereas theory predicts that it should be 4 times greater. This problem is resolved when we examine the effects of the laser on the allowed transition.

The allowed line (4713 Å) shows substantial changes caused by the presence of the laser. Figure VI-33 shows the profile of the helium 4713 Å line. Figure VI-34 shows a profile of the same line when the laser is incident on the plasma. The laser has greatly diminished the intensity of this line, and has also caused the line to become extremely asymmetric. The allowed line is skewed in a manner reminiscent of the satellite (Fig. VI-29). Figure VI-35 shows the integrated intensity of the allowed line

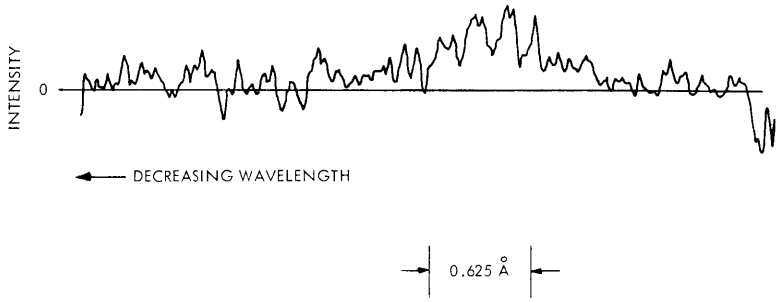

Fig. VI-32. Satellite profile with only 25% laser power incident on the plasma.

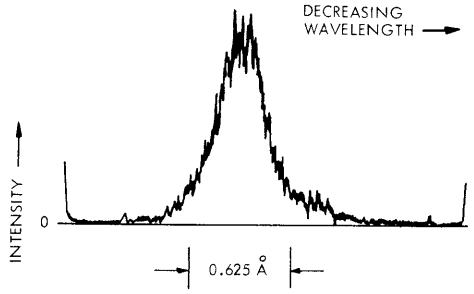

Fig. VI-33.
Profile of 4713 Å line in helium plasma.

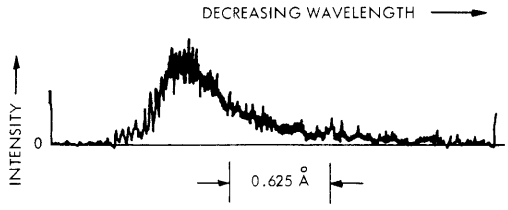

Fig. VI-34.
Profile of 4713 Å line in helium plasma with CO_2 laser incident on the plasma.

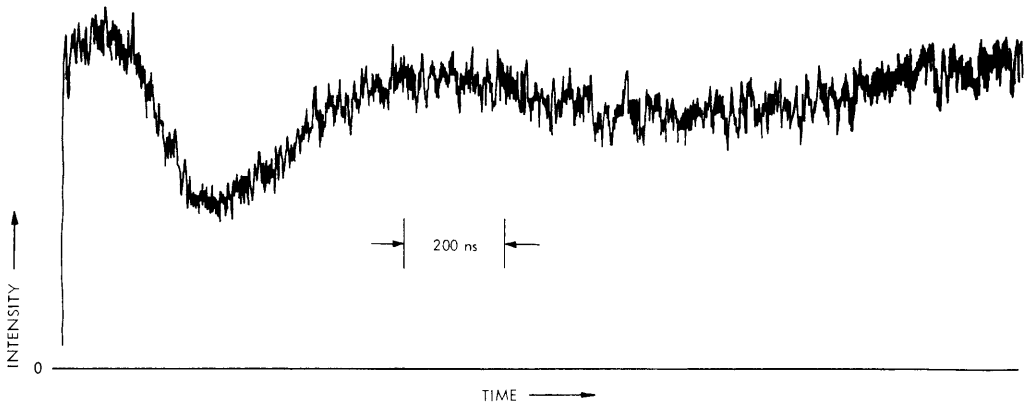

Fig. VI-35. Intensity of 4713 Å line as a function of time. Laser is incident on the plasma.

line as a function of time. It is clear that the intensity of this line is directly affected by the laser field and becomes weaker as the laser gets stronger (cf. Figs. VI-31 and VI-35). These changes are occurring on a time scale that is short compared with the laser halfwidth.

We have computed S_- based on the intensity of the allowed line under the influence of the laser. We find $S_- = 0.03$, which predicts a laser field of approximately 1.2×10^4 V/cm. Approximate laser power measurements predict a field of 1.7×10^4 V/cm, but at present we have only crude measurements that are accurate at best to a factor of 2. When the laser was attenuated 25% (Fig. VI-32) the satellite intensity was diminished 50%, but the intensity of the allowed line nearly doubled, so that $S_- = .0075$, as expected. Thus we see that the changes of the intensity of the allowed line must be included in calculations of S_-.

Several other helium lines also show changes in intensity because of the presence of the laser. Table VI-1 lists these lines and indicates whether the laser caused an

Table VI-1. Laser-induced intensity changes of allowed lines in helium.

Wavelength (Å)	Change	Transition
3188	decrease[1]	4^3P-2^3S
3888	increase	3^3P-2^3S
3964	no change	4^1P-2^1S
4120	decrease	5^3S-2^3P
4387	decrease	5^1D-2^1P
4437	decrease	5^1S-2^1P
4471	no change	4^3D-2^3P
4713	decrease	4^3S-2^3P
4921	no change	4^1D-2^1P
5015	increase	3^1P-2^1S
5047	decrease	4^1S-2^1P
5876	increase	3^3D-2^3P
6678	increase[2]	3^1D-2^1P

[1]Because of low light levels, this change is somewhat uncertain.

[2]This change is small, and thus somewhat uncertain.

increase or decrease in total integrated intensity. All changes were on a time scale commensurate with the width of the laser. Note that not all variations were of the same magnitude; the percentage change of the 4713 A line was several times larger than any

other line examined. The fact that the 4^3S and 4^3P levels are those closest to resonance with the CO_2 laser radiation suggests that some type of laser pumping may be responsible for the intensity changes.

Investigations continue in an attempt to discover the exact nature of all of these interactions. We want to learn how the weakening of the allowed transitions affects the satellite's magnitude, and whether this will prove to be a limit on the detectability of satellites.

References

1. D. Prosnitz, Quarterly Progress Report No. 108, Research Laboratory of Electronics, M.I.T., January 15, 1973, pp. 195-208.
2. M. Baranger and B. Mozer, Phys. Rev. 123, 25-28 (1961).
3. W. S. Cooper III and H. Ringler, Phys. Rev. 179, 232 (1969).

3. CO_2 SHORT-PULSE AMPLIFICATION STUDIES

National Science Foundation (Grant GK-33843)

A. H. M. Ross

We are continuing theoretical studies of short-pulse amplification in high-pressure CO_2 laser amplifiers so that they can be compared with measurements on the E-beam amplifier now in procurement. In our last report[1] we presented numerical solutions for pulse propagation in a two-level medium, including the effects of both homogeneous and inhomogeneous line broadening. Such a model, however, is not appropriate for amplification between rotational states of finite J if pulse durations are shorter than the kinetic collision time. It is also desirable to analyze, in simple approximation, the extraction of energy from the rotational degrees of freedom of the molecules. Therefore we have extended the theory to a model with only two vibrational levels, but with a full rotation spectrum, including orientational degeneracy.

The energy spectrum of our two-level rotor (TLR) model is illustrated in Fig. VI-36. It is a sum of vibrational energy, plus a rigid rotor spectrum, with moment of inertia assumed equal in both vibrational states. (This is not a bad approximation for purposes of calculating Boltzmann factors; in CO_2 the upper laser level has $cB \approx 11,606$ MHz, the lower has $cB \approx 11,697$ MHz. The difference, of course, is important in the calculation of spectra.) The net energy of a state (v, J) is therefore $E_{v,J} = E_v + hcB\,J(J+1)$. Amplification by the CO_2 molecules, at least as envisioned in the present work, takes place between a single pair of the vibration-rotation states illustrated in Fig. VI-36. We assume that collision processes are phase-incoherent, so that we may treat the kinetics of all levels (except those connected by the radiation)

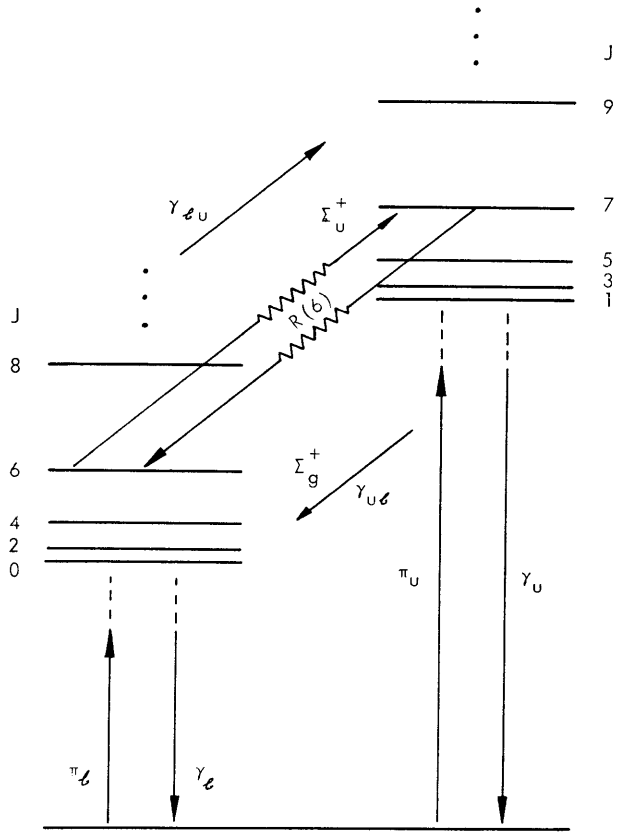

Fig. VI-36. Energy-level structure of two-level rotor model (molecule of point group $D_{\infty h}$).

by phenomenological rate equations.

Schrödinger's equation for the radiation-coupled levels, in terms of the density matrix distribution function[1] for infinite-mass molecules can be written

$$\left(\frac{\partial \rho_{aa}}{\partial \tau}\right)_\zeta = +\frac{i}{2}\left(p_{\lambda o}\tilde{\rho}_{ba}\tilde{\mathscr{E}}_\lambda - \text{h.c.}\right) + \left(\frac{\partial \rho_{aa}}{\partial \tau}\right)_{\text{collision}} \tag{1a}$$

$$\left(\frac{\partial \tilde{\rho}_{ab}}{\partial \tau}\right)_\zeta = +\frac{i}{2}\left(p_{\lambda o}\rho_{bb} - \rho_{aa}p_{\lambda o}\right)\tilde{\mathscr{E}}_\lambda + \left(\frac{\partial \tilde{\rho}_{ab}}{\partial \tau}\right)_{\text{collision}} \tag{1b}$$

$$\left(\frac{\partial \rho_{bb}}{\partial \tau}\right)_\zeta = -\frac{i}{2}\left(p_{\lambda o}\tilde{\rho}_{ba}\tilde{\mathscr{E}}_\lambda - \text{h.c.}\right) + \left(\frac{\partial \rho_{bb}}{\partial \tau}\right)_{\text{collision}}, \tag{1c}$$

where the various ρ are the matrices constituting the total density matrix according to the partitioning

$$\rho = \begin{pmatrix} \rho_{aa} & \tilde{\rho}_{ab}\, e^{+i\kappa_o\zeta} \\ \tilde{\rho}^*_{ab}\, e^{-i\kappa_o\zeta} & \rho_{bb} \end{pmatrix}$$

and $\tilde{\mathscr{E}}_\lambda$ is the dimensionless electric field complex amplitude

$$E_\lambda(\zeta,\tau) = \mathrm{Re}\left[\tilde{\mathscr{E}}_\lambda\, e^{-i(\omega_o\tau-\kappa_o\zeta)}\right] \frac{\hbar}{t_c\left[\mathrm{Tr}\left(p^+_{\lambda' o} p_{\lambda' o}\right)\right]^{1/2}}.$$

We have written the dipole moment matrix as

$$p_\lambda = \begin{pmatrix} 0 & p_{\lambda o}\, e^{+i\omega_o\tau} \\ p^+_{\lambda o}\, e^{-i\omega_o\tau} & 0 \end{pmatrix}.$$

Here, a and b represent the degenerate manifolds of states belonging to the upper laser level and lower laser level, respectively, and ζ and τ are the dimensionless space and time variables introduced in our last report.[1] The wave equation, in slowly varying envelope approximation, becomes

$$\frac{\partial\tilde{\mathscr{E}}_\lambda}{\partial\zeta} = -\alpha\tilde{\mathscr{E}}_\lambda + \frac{i}{2}\tilde{\mathscr{P}}_\lambda,$$

where $\tilde{\mathscr{P}}_\lambda$ is the complex amplitude of the macroscopic polarization,

$$\tilde{\mathscr{P}}_\lambda = 2\ \mathrm{Tr}\left(D^{(\lambda)+}\tilde{\rho}_{ab}\right).$$

We have also normalized the moment matrix

$$p_{\lambda o} = \left[\mathrm{Tr}\left(p^+_{\lambda' o} p_{\lambda' o}\right)\right]^{1/2} D^{(\lambda)}.$$

We have introduced α as a phenomenological loss term to account for "host" medium absorption.

It is instructive to solve these equations in the small-signal approximation. Assuming that ρ_{aa} and ρ_{bb} are both time-independent and proportional to the matrix identity (i.e., all members of the degenerate manifold of states are equally populated), we can easily

find a solution by Fourier transforms

$$\tilde{\mathscr{E}}_\lambda(\zeta, \Omega) = \tilde{\mathscr{E}}_\lambda(\zeta_o, \Omega)\, e^{[g_o(\Omega)-\alpha](\zeta-\zeta_o)}.$$

The small-signal incremental gain is

$$g_o(\Omega) = \frac{1}{6}\left(\frac{n_u}{g_u} - \frac{n_\ell}{g_\ell}\right)\frac{1}{\gamma_o - i\Omega},$$

where n_u and n_ℓ are the total occupancy of the upper and lower levels, respectively, and g_u and g_ℓ are the degeneracies. We have assumed a simple decay for the collision term

$$\left(\frac{\partial \tilde{\rho}_{ab}}{\partial \tau}\right)_{\text{collision}} = -\gamma_o \tilde{\rho}_{ab}.$$

The factor 1/6 in the small-signal incremental gain arises because we are using a correct vector field model; had we assumed scalar fields and a two-level atom we would have found a factor 1/2.

For large-signal solutions it is necessary to solve the rate equations for the other, nonradiatively coupled, levels and to provide expressions for the phenomenological collision terms in the Schrödinger equation (1). If it were necessary to integrate arbitrary initial conditions, or if there were no systematic structure to the rates, the analysis of the problem would stop here, and a very complex set of equations would have to be integrated numerically. Fortunately, some simple approximations allow a description in terms of only two parameters in addition to the density matrix for the radiatively coupled levels. Three assumptions underlie this simplification:

(i) Vibrational relaxation rates are independent of J.

(ii) All collisions thermalize the rotational degree of freedom.

(iii) The system is in a state characterized by thermal equilibrium of the rotational degrees of freedom before arrival of the electromagnetic field pulse.

Both (i) and (ii) are plausible because the spacing between rotational levels is reasonably small compared with $k_B T$. In addition, (ii) has been verified experimentally by Cheo and Abrams.[2] With these assumptions, the rate equations may be written

$$\frac{\partial n_{uJ}}{\partial \tau} = \left(\frac{\partial n_{uJ}}{\partial \tau}\right)_{\text{rad}} - \gamma_u\left(n_{uJ} - n_{uJ}^{(o)}\right) - \gamma_{u\ell}\left(n_{uJ} - \frac{n_{uJ}^{(o)}}{L_o}\, L\right) - \gamma_r\left(n_{uJ} - \frac{n_{uJ}^{(o)}}{U_o}\, U\right) \tag{2a}$$

$$\frac{\partial n_{\ell J}}{\partial \tau} = \left(\frac{\partial n_{\ell J}}{\partial \tau}\right)_{\text{rad}} - \gamma_\ell\left(n_{\ell J} - n_{\ell J}^{(o)}\right) - \gamma_{u\ell}\left(n_{\ell J} - \frac{n_{\ell J}^{(o)}}{U_o}\, U\right) - \gamma_r\left(n_{\ell J} - \frac{n_{\ell J}^{(o)}}{L_o}\, L\right), \tag{2b}$$

where the radiative term is present only for the a and b levels. U and L are the total occupancies of the upper and lower vibrational levels, respectively

$$U = \sum_{J'} n_{uJ'}$$

$$L = \sum_{m} n_{\ell J}$$

with steady-state values U_o, L_o.

With these assumptions, it is clear that the vibration-rotation state populations will be affected by the electric field pulse in the manner illustrated in Fig. VI-37. The dotted

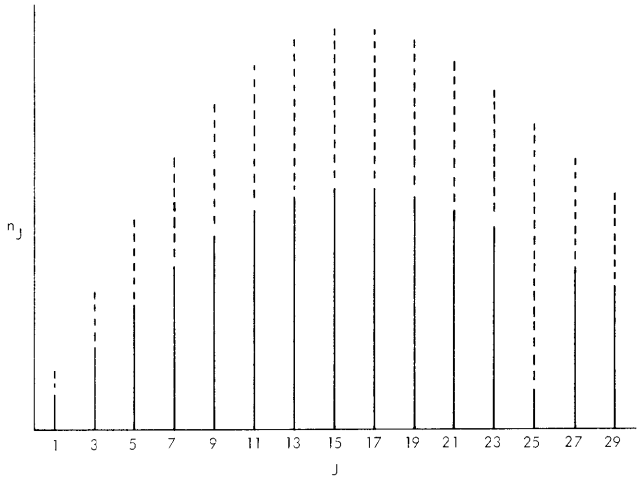

Fig. VI-37. Effect of radiation-induced transitions on upper vibrational state rotational sublevels (affected level, J = 25).

lines represent relative populations in the radiation-free steady state, while the solid lines represent the effect of radiative depopulation of the J = 25 level, which might occur in the presence of P(26) spectral line radiation. States other than the one directly affected by the radiation remain populated in proportion to their steady-state occupancy, but with a different overall amplitude. Of course the level directly affected by the radiation, which is really composed of 2J + 1 sublevels, deviates from that distribution. The degenerate sublevels acquire different populations because of the differing interaction coefficients of the molecules in varying orientations (this is not illustrated in Fig. VI-37). We choose to represent the situation by

$$n_{uJ'} = \left(1 - \sum_{m''} \xi_{m''}\right) f_{J'} U, \quad J' \neq J'_{rad}$$

$$n_{\ell J} = \left(1 - \sum_{m''} \eta_{m''}\right) f_J \, L, \qquad J \neq J_{rad}$$

$$n_{uJ'_{rad}} = \sum_{m'} x_{m'}$$

$$n_{\ell J_{rad}} = \sum_{m} y_m$$

$$x_{m'} = \rho_{uJ'm'; uJ'm'} = \left\{\left(1 - \sum_{m''} \xi_{m''}\right) f_{J'm'} + \xi_{m'}\right\} U$$

$$y_m = \rho_{\ell Jm; \ell Jm} = \left\{\left(1 - \sum_{m''} \eta_{m''}\right) f_{Jm} + \eta_m\right\} L,$$

where the Boltzmann factors are

$$f_J = (2J+1) \frac{2\beta}{\theta} \exp\left[-\frac{\beta}{\theta} J(J+1)\right]$$

$$f_{Jm} = \frac{2\beta}{\theta} \exp\left[-\frac{\beta}{\theta} J(J+1)\right]$$

$$\frac{\beta}{\theta} = \frac{hcB}{k_B T}.$$

The equations of motion for U, L, $\xi_{m'}$, and η_m can be found easily by substitution of the factors above in the rate equations (2) and the Schrödinger equation (1)

$$\left(\frac{\partial U}{\partial \tau}\right)_\zeta = \left(\frac{\partial U}{\partial \tau}\right)_{rad} - \gamma_u (U - U_o) - \gamma_{u\ell} \left(U - \frac{U_o}{L_o} L\right)$$

$$\left(\frac{\partial L}{\partial \tau}\right)_\zeta = \left(\frac{\partial L}{\partial \tau}\right)_{rad} - \gamma_\ell (L - L_o) - \gamma_{u\ell} \left(L - \frac{L_o}{U_o} U\right)$$

$$\left(\frac{\partial \xi_{m'}}{\partial \tau}\right)_\zeta = U^{-1} \left(\frac{\partial x_{m'}}{\partial \tau}\right)_{rad} - \left\{U^{-1} \left(\frac{\partial U}{\partial \tau}\right)_{rad} + \gamma_r + \left(\gamma_u + \gamma_{u\ell} \frac{L}{L_o}\right) \frac{U_o}{U}\right\} \xi_{m'}$$

$$\left(\frac{\partial \eta_m}{\partial \tau}\right)_\zeta = L^{-1} \left(\frac{\partial y_m}{\partial \tau}\right)_{rad} - \left\{L^{-1} \left(\frac{\partial L}{\partial \tau}\right)_{rad} + \gamma_r + \left(\gamma_\ell + \gamma_{u\ell} \frac{U}{U_o}\right) \frac{L_o}{L}\right\} \eta_m.$$

We also need the equation for the "off-diagonal" matrix $\tilde{\rho}_{ab}$. In general, this would depend on the entire matrices ρ_{aa} and ρ_{bb} (remember that $x_{m'}$ and y_m are only the diagonal elements of ρ_{aa} and ρ_{bb}). If we restrict the discussion to a single polarization component, however, the molecular quantization axis may be so chosen that only elements of $\tilde{\rho}_{ab}$ having a particular correspondence between m' and m (one-to-one) are nonzero. If this is the case, then ρ_{aa} and ρ_{bb} remain diagonal for all time, and

the off-diagonal equation can be written

$$\left(\frac{\partial R_{m'm}}{\partial \tau}\right)_{\zeta} = -\gamma_o R_{m'm} + \frac{i}{2} D^{(\lambda)}_{m'm} \tilde{\mathscr{E}}_{\lambda}(y_m - x_{m'})$$

$$R_{m'm} = \tilde{\rho}_{uJ'm';\ell Jm}.$$

Note that this is really indexed by a single index m, since the polarization determines the relationship between m' and m. In this notation, the radiative derivatives needed by the rate equations are

$$\left(\frac{\partial x_{m'}}{\partial \tau}\right)_{rad} = -\left(\frac{\partial y_m}{\partial \tau}\right)_{rad} = \mathrm{Im}\left\{D^{(\lambda)}_{m'm} R^{*}_{m'm} \tilde{\mathscr{E}}_{\lambda}\right\}$$

$$\left(\frac{\partial U}{\partial \tau}\right)_{rad} = -\left(\frac{\partial L}{\partial \tau}\right)_{rad} = \sum_{m'} \left(\frac{\partial x_{m'}}{\partial \tau}\right)_{rad}.$$

The TLR model equations are now being coded for numerical solution, and we expect that they will provide an accurate description of large-signal, fast-pulse propagation in CO_2 amplifiers. In cases where entire vibrational (as opposed to rotational) state populations are substantially affected by the passage of the pulse, we feel it may be necessary to go to a model in which multiquantum excitations of the vibrational states are realistically included. In view of recent measurements[3] of the vibrational equilibration time of the ν_3 mode of CO_2, which showed that it is comparable to the rotational time, feeding of the upper laser level from higher vibrational states may be an important effect, even for fast pulses.

It has come to the author's attention that the lossless pulse solutions in an inhomogeneously broadened two-level medium have now been obtained in closed form by G. L. Lamb.[4, 5]

References

1. A. H. M. Ross, Quarterly Progress Report No. 109, Research Laboratory of Electronics, M. I. T., April 15, 1973, pp. 105-109.
2. P. K. Cheo and R. L. Abrams, Appl. Phys. Letters 14, 47 (1969).
3. I. Burak, Y. Noter, and A. Szöke, IEEE J. Quant. Electronics, Vol. QE-9, No. 5, p. 541, May 1973.
4. G. L. Lamb, Jr., "On the Connection between Lossless Propagation and Pulse Profile" (to be published in Physica).
5. G. L. Lamb, Jr., "Coherent Optical Pulse Propagation as an Inverse Problem" (to be published).